Development of a Novel Gene Therapy

&

Investigation of Synthetic Gene Therapy Delivery Systems

Halli C. Benasutti

A dissertation

submitted in partial fulfillment of the

requirements for the degree of

Doctor of Philosophy

University of Washington

2023

Reading Committee:

Jeffrey S. Chamberlain, Chair

Michael Regnier

Richard Palmiter

Program Authorized to Offer Degree:

Biochemistry

University of Washington

Abstract

Development of a Novel Gene Therapy

&

Investigation of Synthetic Gene Therapy Delivery Systems

Halli C. Benasutti

Chair of the Supervisory Committee:

Jeffrey S. Chamberlain

Department of Biochemistry

Dystroglycanopathies are a family of neuromuscular disorders, in which enzymes that glycosylate the protein dystroglycan and therefore play a key role in muscle structure, have reduced or nonexistent activity. For example, Limb-girdle muscular dystrophy type R9 is caused by a mutation in the *FKRP* gene, that encodes one of various enzymes that glycosylates the muscle membrane protein dystroglycan. The result is muscle degeneration and weakness, and palliative care is presently the only available treatment for dystroglycanopathy patients. We approached the need for treatment from a gene therapy perspective, focusing on two main ideas: 1) the development of a novel AAV gene therapy with which to treat limb-girdle muscular dystrophy type R9, and 2) the evolution of a synthetic nanoparticle with a long-range goal of improving tissue targeting and therapeutic gene delivery. Our research into AAV gene therapy led us to determine that removal of the untranslated regions of the *FKRP* gene increases protein

expression. Following these *in vitro* results, we further verified the restoration of muscle strength and health in a 10-month-old LGMDR9 mouse model. Additionally, potential deleterious effects of AAV-FKRP gene therapy has created controversy in the field, and our data suggest that this is not an issue at the doses and vectors tested, as treated WT mice show no physiological evidence of harmful effects. However, AAVs are unavailable as a treatment for patients with preexisting immunity to the vector, such that alternative gene therapy delivery systems must be considered. Using customizable synthetic nanoparticles bearing a library of surface miniproteins that encapsulate their own mRNA, we selected for desired characteristics (i.e. tissue tropism) over multiple rounds of selection *in vivo*. This genetically coded library consisted of millions of nanoparticles, which we injected into mice for two rounds of *in vivo* selection for binding to specific cell types, such as skeletal muscle. Following each round, we sequenced nanoparticle mRNA in desired tissues, from which we then created a new library to be evaluated *in vivo* again. The results of this suggest common binding moieties in mini-protein binders on the surface of the nanoparticles. The goal is to identify synthetic particles bearing surface proteins that have high affinity for selected tissues that could eventually be used as gene therapy delivery mechanisms for neuromuscular disorders.

TABLE OF CONTENTS:

Table of Figures 8

Acknowledgements 9

Chapter 1. Introduction..... 10

1.1 Gene Therapy 10

1.2 Gene Therapy for Neuromuscular Disorders 11

1.3 Gene Therapy Delivery Systems 12

1.4 Gene Therapy for Limb-Girdle Muscular Dystrophy Type R9 14

1.5 FKRP Mutations and α-Dystroglycan Glycosylation 15

1.6 Nucleocapsid Library Evaluation 17

Chapter 2. Efficacy and muscle safety assessment of fukutin-related protein gene therapy 18

2.1 Abstract 18

2.2 Introduction 19

2.3 Results 24

2.3.1 Removal of the 5' untranslated regions from the FKRP cDNA increases protein expression 24

2.3.2 A6.C8hF treated mice show significantly improved grip strength in a dose- and time-dependent manner 26

2.3.3 Exercise capacity of mice treated with high dose is significantly improved 28

2.3.4 High dose A6.C8hF partly ameliorates the dystrophic respiratory pattern and endurance capacity in $FKRP^{P448L}$ mice 29

2.3.5 Mutant mice treated with A6.C8hF have decreased muscle degeneration, improved fiber size distribution, and decreased creatine kinase levels 31
2.3.6 AAV injection leads to non-uniform FKRP expression in wild type and treated $FKRP^{P448L}$ mice 32
2.3.7 Wild type animals treated with AAV-FKRP vectors display normal muscle physiology 34
2.4 Discussion 39
2.5 Materials & Methods 43

Chapter 3. In Vivo Evolution of Synthetic Self-Assembling Nucleocapsids for Targeted Therapeutic Delivery 53
3.1 Abstract 53
3.2 Introduction 53
3.3 Results 56
3.3.1 *In vivo* library selection of synNCs with surface mutations and miniprotein binders to alter biodistribution..... 56
3.3.2 Identification of enriched synNCs in select tissues..... 58
3.3.3 Biodistribution of most enhanced sequences in heart and skeletal muscle..... 59
3.4 Discussion 62
3.5 Materials & Methods 65

Chapter 4. Conclusions 68

4.1 Summary of findings regarding AAV-FKRP gene therapy in WT and mutant mice 68

4.2 *In vivo* evolution of synthetic nucleocapsid libraries for enhanced tissue targeting 70

Chapter 5. Supplemental Figures 71

Chapter 6. References 72

Table of Figures

Figure 2.1: Removal of the *FKRP* 5'- and 3'-UTRs increases FKRP expression 24

Figure 2.2: Changes in forelimb and hindlimb grip strength over time..... 25

Figure 2.3: Energetics of exercise performance 27

Figure 2.4: The effects of exercise impact training in the high-dose experiment. 29

Figure 2.5: Morphological changes induced by *FKRP* delivery. 30

Figure 2.6: Immunofluorescent staining reveals mosaic expression of exogenous FKRP 32

Figure 2.7: Whole-body and isolated limb physiology of wild-type mice treated with AAV-hFKRP..... 35

Figure 2.8: Cardiac hemodynamics and skeletal muscle mechanics following AAV delivery to wild-type mice 37

Figure 3.1: Schematic of experimental process for *in vivo* evolution of nucleocapsid library ... 55

Figure 3.2: synNC sequences enriched in tissue over lowest enrichment in liver 57

Figure 3.3: Biodistribution and sequence enrichment in tissues 60

Acknowledgments

In sitting down to write this, I must admit that of all the writing that culminates in this thesis, this section has been the most difficult part. Despite my training as a science communicator, it is difficult for me to express my gratitude in words. So many amazing people deserve acknowledgment. I am so proud of the human I have become through this experience; she's badass, and worthy, and she's changing this goddamn world. It's all thanks to you. I'd list your names, but I fear they wouldn't come close to fitting on this page. Many of you will likely never read this, but if you are reading this, then you should know you are one of these people.

Thank you.

So, so much.

CHAPTER 1: Introduction

1.1 Gene Therapy

Gene therapy is a therapeutic that utilizes and/or affects genes, which are segments of DNA that code for specific proteins within a cell. Specifically, these therapeutics are being developed to treat genetic disorders, which are diseases caused by mutations in the patient's genome. These mutations can have any number of effects on patients, depending on the type of mutation and the gene in which the mutation occurs. Gene therapy works to restore the function of the mutated gene or provide gain-of-function genetic modifications in a variety of ways. Therefore, it offers a new and exciting tool to treat these mutations and thus the patients that are affected by them. For example, Zolgensma® is a gene therapy for Spinal Muscular Atrophy Type I (SMAI), in which babies experience muscle weakness resulting in respiratory issues, problems swallowing, and the inability to cough. SMAI is caused by a mutation in the *SMN1* gene, which makes survival motor neuron protein (SMN), and when mutated, results in degeneration of motor neurons. This causes muscle cells to degenerate, resulting in the shoulder, pelvic, and thigh atrophy that is so characteristic of this disease. Zolgensma® is a virus-vector based gene therapy that is designed to introduce the unmutated form of the *SMN1* gene to muscle cells to restore SMN function and rescue the disease phenotype.

The delivery systems, transgene design and mechanism of action, dose, and promoter sequence used provide a vast array of gene therapy development that we can explore to create the most powerful, targeted therapeutics for these many diseases. These components comprise the basic foundational tools of building a gene therapy, and each component has an entire field of dedicated research for each disease to which a gene therapy is being developed and applied. And the variety within these components continues to grow as researchers further develop the field.

As variety in patient genotypes and phenotypes arise, we can work to treat each patient in the most successful and safe manner.

1.2 Gene Therapy for Neuromuscular Disorders

One application of gene therapy is to treat neuromuscular disorders. These comprise a wide range of both inherited and acquired diseases ranging from nerve damage caused by diabetes (diabetic neuropathy) to extensive muscular fiber destruction (necrotizing myopathy). The correlation between all these diseases is that they affect the peripheral nervous system, and the motor and sensory neurons within this system are unable to communicate with the rest of the body. The predominant symptom of these diseases is progressive muscle weakness. Two subsets of the heritable muscular disorders are congenital myopathy and muscular dystrophy, and it is these groups of diseases to which gene therapy research has been rigorously applied.

The Chamberlain lab focuses on developing gene therapies for specific types of muscular dystrophy. One of these types is Duchenne muscular dystrophy (DMD), one of the most common genetic disorders. It is caused by a mutation in the *Dystrophin* gene, causing the dystrophin protein to be non-functional. This then affects muscle cells and their ability to synchronize during a muscle contraction, initiating muscle fiber degeneration. The result is progressive and severe muscle wasting resulting in a patient life-expectancy of ~35 years with palliative care. The Chamberlain lab has been the leader in advancing gene therapies to treat DMD. The *Dystrophin* gene is the largest known gene in the human body[(1)] and therefore poses a significant obstacle to gene-therapy delivery. Research from the Chamberlain lab has effectively miniaturized the *Dystrophin* gene,[(2)] and it is now being used in clinical trials of gene therapy for

DMD (ClinicalTrials.gov Identifier: NCT03368742). This lab continues to explore and develop new transgenes that are more successful in the treatment of muscular dystrophies.[3] DMD is also one of a variety of neuromuscular disorders that are a focus of this lab, and all of these novel gene therapies being developed necessitate the development of optimally effective delivery systems to maximize treatment efficiency.

1.3 Gene Therapy Delivery Systems

There are currently over 25 other gene therapies that have been approved for use by the FDA, treating diseases from multiple myeloma to cartilage defects of the knee to hematopoietic disorders. And that number continues to grow. These therapeutics also range in the actual function and type of gene therapy as well. For example, antisense oligonucleotides are synthetic, short, single-stranded oligonucleotide sequences that can alter RNA processing and thus protein expression;[4] they have been approved for use in treating Duchenne muscular dystrophy (Vyondys 53™) and spinal muscular atrophy (Spinraza®). There are also viral-vector mediated therapeutics such as Zolgensma®, in which *SMN1* is delivered to cells via an adeno-associated viral vector (AAV). This delivery mechanism is the most common in the field of gene therapy, because these viral capsids have unique abilities to deliver their cargo directly into a cell's nucleus. Once the single-stranded DNA tthat he AAV carries anneals to a second strand, it can be transcribed by the host cell,[5] restoring protein expression and rescuing the phenotype.

However, AAV use is limited by safety, carrying capacity, and tissue tropism, all of which significantly affect the success of the gene therapy. As AAV are naturally occurring viruses, many people have been previously infected by these viruses, and therefore have pre-

existing immunity to the capsid. Liver and spleen are the principal sites of natural AAV infection, and a large proportion of therapeutic capsids end up in the liver. This poses a significant problem because patients that have antibodies to AAVs and are treated with AAV gene therapy will likely experience a severe immune response. Currently, patients are put on immunosuppressants to avoid this likely outcome; however, immunosuppressants also pose a considerable health risk. AAVs are also limited to carrying 4.5 to 5 kilobases (kb) of DNA.[6] Therefore, as the *Dystrophin* gene is 2,200 kb, it was necessary to develop a shorter, but still functional, version of the gene. A mini-dystrophin gene (<4kb) was developed by removing non-critical spectrin-like repeats in the rod domain. Dystrophic *mdx* mice that expressed this gene showed a restoration of calcium currents in skeletal muscle.[7] Mini-dystrophin likewise transduces myogenic cells quite stably, persisting for upwards of 6 months and preventing muscle fiber degeneration.[8] Finally, tissue tropism additionally limits the use of AAVs for gene therapy, as many serotypes are multi-tissue specific and most of the virus ends up in the liver.

Presently, there are 11 AAV serotypes that have been identified and are used for their differing tissue tropism and cell-targeting. A widely utilized serotype is AAV2, which effectively targets the kidneys, eyes, and central nervous system. These serotypes can be further broken down into pseudotypes, which are AAVs that are a combination of the initial 11 serotypes' genome and capsid. So AAV2/5 is the AAV2 genome encapsulated in the AAV5 capsid, which together improve neuron targeting and liver de-targeting.[9] Thus, the library of serotypes remains rather large, with lots of room for alterations and improvement.

1.4 Gene therapy for LGMDR9

In chapter 2 of this dissertation, I will cover the research into the development, implementation, and safety of a fukutin-related protein (FKRP) gene therapy for Limb-girdle muscular dystrophy type R9 (LGMDR9). Development of the FKRP antibody and transgene design were performed by Dr. Jane Seto. Studies on FKRP^{P448L} LGMDR9 mouse model were performed in the Rodgers lab at Washington State University, Pullman, WA. This mutant mouse recapitulates the symptoms of LGMDR9 similar to that in humans, and likewise contains one of the homozygous mutations most commonly seen in patients with LGMDR9. I performed extensive physiological analyses and safety assessment of this novel transgene using new and evolved AAVs. The manuscript was written by me, with input from Dr. Jeff Chamberlain and Dr. Buel Rodgers.

1.5 FKRP Mutations and α-Dystroglycan Glycosylation

FKRP is a type II transmembrane Golgi-resident glycosyltransferase and it post-translationally modifies α-dystroglycan (α-DG). It colocalizes to the golgi body with α-DG, however, evidence suggests that some FKRP mutations alter the enzyme's cellular sublocalization,[10, 11] indicating that FKRP structure is critical to its function and transport. When functional FKRP reaches the golgi body, it uses a specific cytidine diphosphate (CDP)-ribitol to transfer Rbo5P onto α-DG,[12] which is thought to be critical for α-DG binding to laminin because of the N- and O-mannosylation. Specifically, the O-mannosylation of α-DG acts as a receptor for cell-extracellular matrix adhesion, and the Rbo5P provided by FKRP results in the extension of this O-linked glycan chain.[13] The end of this chain is then capped with a matrix-binding heteropolysaccharide synthesized by like-acetylglucosaminyltransferase (LARGE).[14] In fact,

there are at least 20 known enzymes that contribute to the complete glycosylation of α-DG, each sequentially adding to or modifying a component on the glycan chain.[15] Disruption of any portion of this post-translational processing results in lack of α-DG binding to laminin,[16] causing various forms of recessive muscular dystrophy. Thus, much of the gene therapy work focused on treating LGMDR9 works with the enzymes that are characterized by their effects on α-DG glycosylation.

Glycosylation is a common post-translational modification that helps to dictate the stability and conformation of fully functional proteins, as well as provides transport signals, and adhesion and anchoring mechanisms. There are two primary glycoforms that have been studied regarding protein glycosylation, N-linked and O-linked. N-linked carbohydrates are linked specifically via an asparagine and an N-acetylglucosamine, whereas O-linked glycans, as in the case of α-DG, are covalently bonded N-acetylgalactosamine to a serine or a threonine on the protein surface. O-linked glycans serve additional purposes such as guiding immune cell trafficking and regulating cellular metabolism, and the glycans themselves are synthesized via the manipulation of chemical moieties which mask hydroxyl groups to prevent them from interacting with other chemicals. This allows for chemical alteration of the exposed hydroxyl group, which then serve as a point for further manipulation and addition. O-mannosylation, the first transfer of a glycan onto the surface of α-DG, occurs in the endoplasmic reticulum, then the protein is transported to the Golgi body to continue the glycosylation process by FKRP and other glycosyltransferases.

It is accepted that abnormalities in the Rbo5P glycosylation pathway of α-DG result in dystroglycanopathies. As CDP-Rbo5P is the donor substrate FKRP uses to add Rbo5Ps in tandem onto α-DG,[17] it may be assumed that mutations in FKRP that disrupt this pathway have

effects on the CDP-Rbo5P biosynthesis abilities of FKRP. Recent data has shown that FKRP activity may be dependent on the formation of a protein complex comprised of FKRP, fukutin, and transmembrane protein 5 (TMEM5).[18] This complex retains each individual protein's enzymatic activities, and mutations in FKRP could actually prevent formation of this complex and thus loss of the complex, not enzymatic activity, could be the cause of LGMDR9. This could explain why FKRP mutants are still enzymatically active yet glycosylate at decreased levels.

Because of these unknowns combined with FKRP being only one of various enzymes that perform tasks related to the glycosylation of α-DG, many labs have started investigating the roles of these other components and their potential application in treating various dystroglycanopathies. For example, evidence has shown that overexpression of LARGE rescues the LGMDR9 phenotype,[19] but this may be a dangerous approach as other data that shows that LARGE upregulation in the absence of skeletal muscle FKRP worsens muscle pathology.[20] Since FKRP homozygous null mutations are embryonic lethal, it suggests that even mutant FKRPs still retains partial enzymatic activity. Additionally, evidence of 'revertant' myofibers expressing glycosylated α-DG implies partially functional mutant FKRPs.[21] It has also been shown that overexpression of mutant FKRP ameliorates the LGMDR9 phenotype by restoring functional glycosylation of α-DG,[22] suggesting that more creative approaches can be taken to treat LGMDR9 that may not be limited by issues of overexpression-facilitated toxicity.

1.6 Nucleocapsid Library Evaluation

The third chapter is the culmination of my work with Audrey Olshefsky in the King Lab at the University of Washington, Seattle, WA. Together, we used a synthetic, self-assembling nucleocapsid system to create a library of capsids bearing millions of surface mutations and small protein binders. We then evaluated this library *in vivo* to identify sequences that increase tissue specificity. The library was created by Audrey, and each round of *in vivo* selection and analysis we performed together. This study involved 2 rounds of selection, culminating in an examination of the biodistribution of enriched cardiac-, skeletal muscle-, liver-, spleen-, lung-, kidney-specific sequences.

CHAPTER 2: Efficacy and Muscle Safety Assessment of Fukutin-Related Protein Gene Therapy

Chapter 2 is adapted with minimal modification of H Benasutti, JW Maricelli, J Seto, J Hall, C Halbert, J Wicki, L Heusgen, Purvis, M Regnier, DC Lin, BD Rodgers, JS Chamberlain. Submitted to Molecular Therapy-Methods & Clinical Development.

2.1 ABSTRACT:

Limb girdle muscular dystrophy type R9 (LGMDR9) is a muscle-wasting disease that begins in the hip and shoulder regions of the body. This disease is caused by mutations in Fukutin-related protein (FKRP), a glycosyltransferase critical to maintaining muscle cell integrity. Here we investigated potential gene therapies for LGMDR9 containing an FKRP expression construct with untranslated region (UTR) modifications. Initial studies treated an aged dystrophic mouse model ($FKRP^{P448L}$) with retro-orbital injections of adeno-associated viral vector serotype 6 (AAV6). Grip strength improved in a dose- and time-dependent manner and injected mice also exhibited fewer central nuclei, larger muscle fibers and 3- and 5-fold lower serum creatine kinase levels compared to non-injected $FKRP^{P448L}$ mice. Treatment also partially stabilized the respiratory pattern during exercise, significantly reduced the accumulation of motivational shocks and therefore improved treadmill running and partially protected muscle from exercise-induced damage. Western blotting of C2C12 myotubes using a novel rabbit antibody confirmed heightened translation with the UTR modifications, striated muscle transgene expression and a trend towards improved exercise training on native FKRP levels. We then explored the question of FKRP toxicity in wild-type mice using high doses of two additional muscle-tropic capsids: AAV9 and AAVMYO1. No toxic effects were detected with either therapeutic, as force development of different skeletal muscles, grip strength, running performance and cardiac

contractility were all unaffected. These data support the feasibility of an AAV-mediated gene therapy to treat LGMDR9 patients.

2.2 INTRODUCTION:

Dystroglycanopathies are a family of muscle disorders (> 20)[23] that are caused by altered glycosylation of α-dystroglycan (α-DG), a peripheral membrane protein located on the extracellular side of the sarcolemma that normally binds to laminin. The laminin-α-DG association is a crucial portion of the dystrophin-glycoprotein complex (DGC), which provides a mechanical link between the intracellular actin cytoskeleton and the extracellular matrix. The DGC enables the lateral transmission of forces from within myofibers,[24] allowing the muscle bundle to contract in unison and preventing cellular damage by internally maintained contractile energy. More than 11 glycosyltransferases are known to post-translationally modify α-DG,[25] working sequentially to build long glycan chains onto the protein. One such glycosyltransferase, Fukutin-related protein (FKRP), catalyzes the transfer of ribitol 5-phosphate to a phosphorylated O-mannosyl trisaccharide on α-DG, but only after Fukutin has added a ribitol 5-phosphate to the growing chain. These sequential modifications lead up to the addition of a repeating glucuronic acid and xylose chain[23] that serves as the laminin binding domain of α-DG.

Altered α-DG glycosylation severely disrupts the DGC mechanics, leading to fragile sarcolemma membranes and muscular dystrophy. These resulting dystroglycanopathies are the primary cause for several forms of congenital muscular dystrophy as well as multiple limb-girdle muscular dystrophies. Limb-girdle muscular dystrophy type R9 (LGMDR9, previously LGMD2I) is one of the most common of these diseases. It is an autosomal recessive disorder

caused by mutations in the *FKRP* gene which also can lead to congenital muscular dystrophy (MDC1C), Walker-Warburg syndrome (WWS) and muscle-eye-brain disease (MEB). Our study is focused on developing treatment options for LGMDR9, although the results will also be relevant to the other, less prevalent FKRP disorders. LGMDR9 is slowly progressive, but patients still experience symptoms such as muscle weakness, muscle cramps, hypertrophy, joint contractures, and ultimately severe cardiomyopathy and respiratory issues. The age of LGMDR9 onset varies, with a spectrum of symptoms presenting in relation to specific mutations in FKRP.[26] For example, affected LGMDR9 patients are often wheelchair-dependent by 25 years after age of onset. Diagnoses are typically made based on elevated serum creatine kinase (CK) levels and proximal muscle weakness followed by genotyping. There is no cure for LGMDR9, and treatments are limited to temporary symptom amelioration.

LGMDR9 is often due to heterozygous and homozygous mutations in the 1.5 kb coding region of the *FKRP* gene, the most common of which is 826C>A (L276I).[8] There is a strong genotype-phenotype correlation for this mutation with compound heterozygous patients displaying a more severe phenotype than homozygous patients.[27] Another common mutation is 1343C>T (P448L), and both mutations interfere with the transfer of FKRP from the endoplasmic reticulum to the Golgi apparatus.[28] As FKRP is a post-translational glycosyltransferase, mislocalization of this enzyme leads to decreased glycosylation and half-life, and results in increased targeting of α-DG by the proteosome.[11] Additionally, other insertion, deletion, missense, and nonsense mutations have been reported in patients, though less commonly than the L276I and P448L point mutations. Interestingly, FKRP-null mutations are embryonic lethal,[29] which explains why all patients genotyped to date have at least one mutant allele that leads to

expression of a presumably partially functional protein. These and other data[22] suggest that most, if not all, mutant FKRP enzymes found in patients still retain some enzymatic activity.

Developing approaches for gene therapy of LGMDR9 have been promising. However, inconsistent vectors, mouse age, genotype, and transgene have resulted in contradictory toxicity evidence associated with FKRP-overexpression. For example, recent data have shown that adeno-associated viral vector (AAV) -mediated systemic delivery of FKRP can significantly ameliorate the dystrophic phenotype in a murine disease model, the $FKRP^{P448L}$ mouse.[30, 31] By contrast, studies with a different model, the $FKRP^{L276I}$ mouse, suggest that muscle pathologies are exacerbated as central nucleation, endomysial fibrosis and macrophage infiltration all increased with treatment.[32] Phenotypic differences in the mouse models are noticeable as $FKRP^{P448L}$ mice reasonably recapitulate LGMDR9[33, 34] while the $FKRP^{L276I}$ mouse displays a mild or less pronounced phenotype.[35, 36] Mouse age varied widely across the studies and the regulatory cassettes used in the various studies similarly differed, as some groups used the strong and ubiquitously expressed CMV (human cytomegalovirus immediate early enhancer plus promoter) or CB (CMV enhancer/chicken β-actin promoter) cassettes while others used a muscle-specific creatine kinase (CK7) cassette. The use of the mouse vs. the human FKRP cDNA also varied between studies, as did doses that ranged from $2x10^{12}$ vg/kg to $6x10^{13}$ vg/kg. The ability of gene therapy to treat LGMDR9 as well as its durability are also significantly dose-dependent, with lower doses displaying shorter-term, but still significant effects.[37]

Moreover, only one test of systemic muscle function has been performed on $FKRP^{P448L}$ mice receiving FKRP gene therapy, a treadmill exhaustion assay that, although useful, provides limited metrics for analysis. Other tests of systemic muscle function include running wheels for voluntary exercise and treadmills with respiratory chambers for assessing metabolic rate during

forced exercise,[38] all of which are recommended assessments for preclinical studies with dystrophic mice.[39, 40] Quantifying metabolic rate through indirect calorimetry assesses the combined functional integrity of both skeletal and cardiac muscle and differs from plethysmography. This latter measure of ventilation reflects diaphragm function only and has little effect on metabolic rate.[41-45] Exercise-based assessments mimic those often used to assess dystrophic patients in the clinic (e.g., 6-minute-walk test) and can be used to exacerbate the dystrophic phenotype in preclinical studies. [46-49]

Therapeutic delivery method is yet another critical component that must be considered in the development of the safest possible therapeutic for LGMDR9 and related CMDs. Increased gene expression is often a critical part of gene therapy, as therapeutics are limited by the immune responses associated with high doses of AAVs in human patients. For example, the issue of systemically administered AAVs and the accompanying liver toxicity seen in clinical trials[50, 51] remain a barrier moving forward. Therefore, an ideal treatment would maximize gene expression while minimizing the AAV dose. The latest advancements in AAV vector designs have led to increased targeting and gene expression in specific tissues. The development of these capsid variants that enable muscle-specific gene delivery may alter dosing thresholds and therapeutic efficacy,[52-54] and need to be examined in relation to current vectors used in the clinic. One such novel AAV capsid has been named AAVMYO1 for its myotropic properties, and has been shown to increase efficiency and specificity in heart, diaphragm, and skeletal muscle.[53] These new developments not only address the issue of myotropism but also decrease liver-tropism, which will be critical to avoid the issues of innate immunity, and which will affect the success of gene therapies using high dose AAV vectors.

While it has been shown that FKRP gene therapy is generally an effective treatment in mouse models for LGMDR9,[32, 37] there has been little focus on transgene designs. Transgene optimization provides a tool to improve efficacy and lower necessary treatment doses. One such successful method of increasing gene expression was demonstrated in samples from cystic fibrosis patients.[55, 56] The untranslated region (UTR) of the CFTR gene contains regulatory elements that decrease translation; in this case, the formation of a secondary structure in the 5' UTR post-transcriptionally regulates CFTR via cooperative regulatory effects. Thus, removal of the 5' UTR ultimately increased CFTR expression. We discovered evidence of potential secondary structures in the untranslated regions of FKRP mRNA.[57] One particularly relevant structure is an RNA G-quadruplex (RGQ), a stable secondary mRNA configuration associated with the inhibition of translation.[58, 59] Repeats of a (CGG) motif in the 5'UTR of FKRP are suggestive of an RGQ, and further investigation into UTR regions may provide a tool for tunable gene expression (for FKRP and other genes).

The current study tested the dose-dependent efficacy of a novel FKRP gene therapeutic. This particular therapeutic differed from the vectors previously tested[30, 32, 35] as it used AAV6 instead of AAV9, as well as a miniaturized mouse muscle creatine kinase enhancer/promoter (*CK8e*) that is uniquely active in striated muscle (AAV6-Ck8e-humanFKRP, A6.C8hF).[3, 60-65] Furthermore, we examined a range of mouse ages and assessed systemic muscle function using a customized treadmill protocol.[49] Our results suggest that delivering a small FKRP cDNA to $FKRP^{P448L}$ mice significantly improves different aspects of striated muscle structure and function in a dose-dependent manner. However, even the higher dose tested here did not completely restore muscle function to levels seen in wild-type mice. Finally, to address the issue of potential FKRP toxicity, we explored whether overexpression of FKRP in wild-type mice affected muscle

physiology. These studies delivered the small FKRP cDNA using multiple doses of vectors pseudotyped with capsids from AAV6,[66] AAV9,[67] and the newer AAVMYO1.[52] Cardiac and muscle physiology did not identify any adverse functional affects due to the exogenous FKRP in wild type mice.

2.3 RESULTS:

2.3.1 Removal of the untranslated regions from the FKRP cDNA increases protein expression.

To explore FKRP expression, we initially generated rabbit polyclonal antisera (named Ab607) against a conserved fragment of the C-terminus of mouse and human FKRP (see methods). To verify the utility of the antisera after affinity-purification, C2C12 myotubes were transduced with $1x10^{12}$ vg, $1x10^{11}$ vg, or $1x10^{10}$ vg of AAV6-CK8e-mFKRP-FLAG (the murine *Fkrp* cDNA with a C-terminal FLAG-tag). Cell lysates revealed co-immunoreactivity with the FKRP and FLAG antibodies and provided confirmation of FKRP production by the AAV6-CK8e-FKRP vector (Fig. 2.1A). To maximize protein expression, we searched for potential inhibitory sequences in the *FKRP* untranslated regions. Sequence analysis suggested there may be regulatory secondary mRNA structures, so both UTRs were removed from the *Fkrp* cDNA (A6.C8mF). Note, however, that CK8e, which is present in all these vectors, carries 49 bp from the mouse CKM 5' UTR and that the polyA sequence used was also identical in all vectors (see methods). The effects of these modifications were then compared *in vitro* by transducing C2C12 myotubes with vectors either carrying or lacking both the *Fkrp* 5' and 3' UTRs. Western analysis with Ab607 showed a notable increase in FKRP expression upon the removal of the UTRs (Fig. 2.1B). This vector was then tested *in vivo* via intramuscular injections into the tibialis anterior (TA) of wild-type mice ($1x10^{11}$vg/muscle).[66]

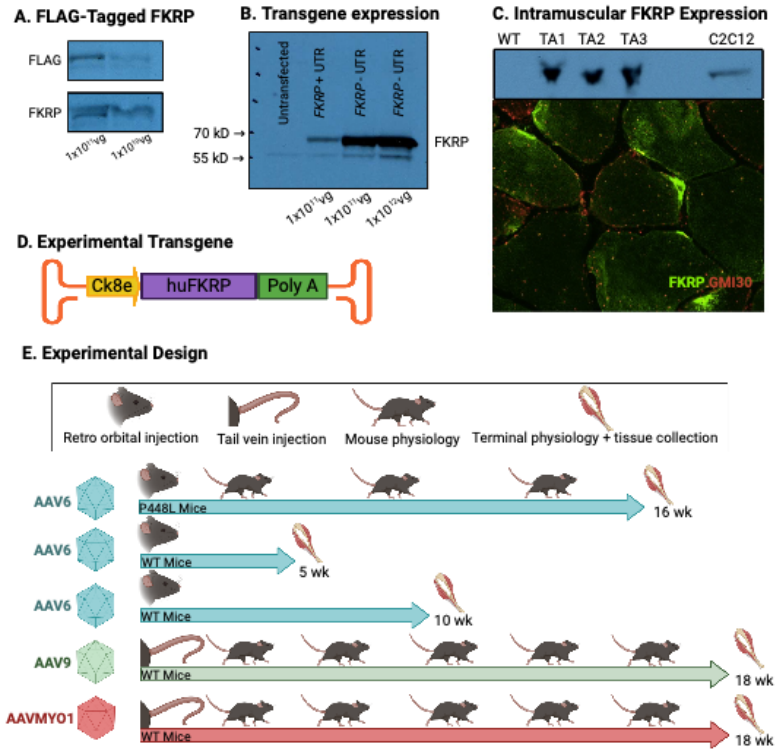

Figure 2.1: Removal of the *FKRP* 5'- and 3'-UTRs increases FKRP expression. A, Cell lysates from differentiated C2C12 myotubes transduced with either $1x10^{11}$ or $1x10^{10}$ vector genomes (vg) of A6.C8mF-FLAG to verify vector expression of mouse *FKRP* (mFKRP). Labels on the left indicate antibody target (FKRP, Ab607; FLAG, FLAG-HRP, Sigma F7425). **B,** FKRP levels in myotubes transduced with untagged AAV6-Ck8e-mFKRP (+UTR) and AAV6-Ck8e-mFKRP (-UTR). **C,** Upper: FKRP expression in tibialis anterior (TA) muscles of wild-type mice injected IM with $1x10^{11}$ vg AAV6-Ck8e-mFKRP (-UTR) relative to an untreated wild-type mouse and C2C12 myotubes transduced with $1x10^{12}$ vg of same vector; Lower: Immunostaining of wild-type tibialis anterior muscle injected with AAV6-CK8e-mFKRP. FKRP, green. Golgi, red (GMI30). **D,** Schematic illustration of the AAV-CK8e-humanFKRP (hFKRP)construct used in these studies. **E,** This transgene construct was expressed from vectors pseudotyped with capsids from AAV6 (A6.C8hF), AAV9 (A9.C8hF), or AAVMYO1 (AM.C8hF). Wild-type and $FKRP^{P448L}$ mutant mice were then treated and tested at various timepoints post-injection to identify potential physiological and histological changes. WT, wild type; P448L, $FKRP^{P448L}$.

Analysis of injected muscles revealed FKRP expression by western blot as well as mosaic distribution of the protein throughout the injected muscles (Fig. 2.1C). While some FKRP immunostaining colocalized with GIM130 in the Golgi, much of the exogenous protein was diffusely localized (see also Fig. 2.6), as has previously been observed by others.[32, 35]

To explore potential deleterious effects from high levels of exogenous FKRP expression, we generated a similar vector that expressed the human FKRP (also lacking the *FKRP* 5' and 3' UTRs). This CK8e-hFKRP construct was encapsulated into AAV6 (A6.C8hF), AAV9 (A9.C8hF), or AAVMYO1 (AM.C8hF) vectors and tested in various strains of mice via systemic delivery (Fig. 2.1D).[68] The first cohort, comprised of FKRP^{P448L} mutant mice, was injected with A6.C8hF at doses of $1.5x10^{13}$ and $1.5x10^{14}$ vg/kg and analyzed with a variety of tests of muscle strength and exercise performance at different timepoints (Figs. 2.2-2.6).

2.3.2 A6.C8hF treated mice show significantly improved grip strength in a dose- and time-dependent manner. Ten-month-old FKRP^{P448L} mutant mice were injected with different doses of A6.C8hF (saline, $1.5x10^{13}$, and $1.5x10^{14}$ vg/kg) and monitored alongside age-matched wild-type controls. The purpose of using older mice was to address the effect of treatment in older mice with a more advanced phenotype. Forelimb grip strength of age matched wild-type, untreated and treated FKRP^{P448L} mice was measured at 4-, 8-, 13-, and 16-weeks post-injection. Absolute forelimb grip strength progressively increased in a dose-dependent manner among treated mice but did not change in wild-type or untreated FKRP^{P448L} mice (Fig. 2.2A).

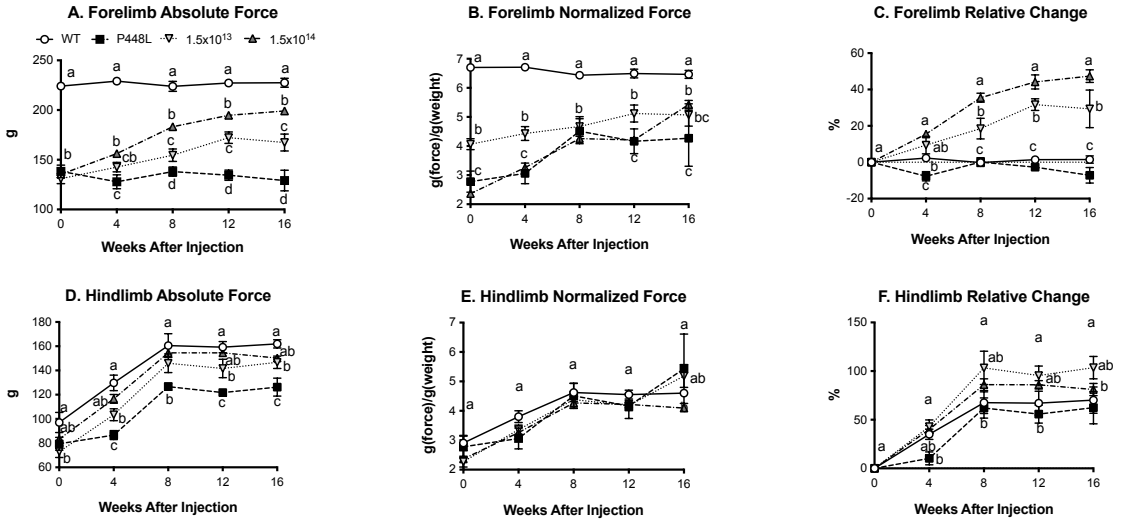

Figure 2.2: Changes in forelimb and hindlimb grip strength over time. A-C, Forelimb grip strength and **D-E,** hind limb force of wild-type mice and of mutant mice injected with saline (P448L), $1.5x10^{13}$, or $1.5x10^{14}$ vg/kg A6.C8hF. A **& D,** Forelimb grip strength over time. **B & E,** absolute force was normalized to body mass. **C & F,** Percent change from absolute force measurements at baseline. All mice were 10 months old at baseline. Significant differences between treatment groups at a given time point are indicated by different letters whereas shared letters indicate no difference. WT, wild type; P448L, untreated. (n=4-5)

Compared to untreated $FKRP^{P448L}$ mice, 4 months of treatment with low and high dose vector restored strength to approximately 40% and 70%, respectively, of wild-type levels, although the rate of improvement appeared to level off after 3 months in low dose mice. Normalizing these data to body weight (Fig. 2.2B) can confound the results however, because : (i) the low-dose group included both males and females whereas the high-dose group included only males and (ii) body weight varied greatly among aged mice and was therefore a poor normalizing factor.[69] We therefore measured the individual percent change over time to remove the data-biasing effects of sex and age, and validated the dose-dependent and temporal increase in grip strength demonstrated by plotting relative change (Fig. 2.2C). Upon examination of the relative force change over the course of the 16 weeks, we observed that relative strength increased significantly in a dose-dependent manner.

Hindlimb grip-strength measurements are often highly variable until mice become accustomed to the assay, although habituation over time is also a concern. Indeed, grip-strength absolute force increased in all groups, including untreated $FKRP^{P448L}$ mice, over the first two months (Fig. 2.2D). Absolute force was also similar in treated mice regardless of dose and at all time points. However, treated mice were also stronger than untreated by this measure, while grip strength in both wild-type and high dose mice was similar. Tracking the relative change among individuals indicated a treatment effect for one or both doses at all time points (Fig. 2.2F), although

there were again no clear differences between doses. These results suggest that despite the innate variability of the assay, treatment with A6.C8hF increased hindlimb grip strength in aged mice.

2.3.3 Exercise capacity of mice treated with high dose is significantly improved. Impact training had a beneficial effect in wild-type mice and increased VO_2max by almost 10% (Fig. 2.3A & B).

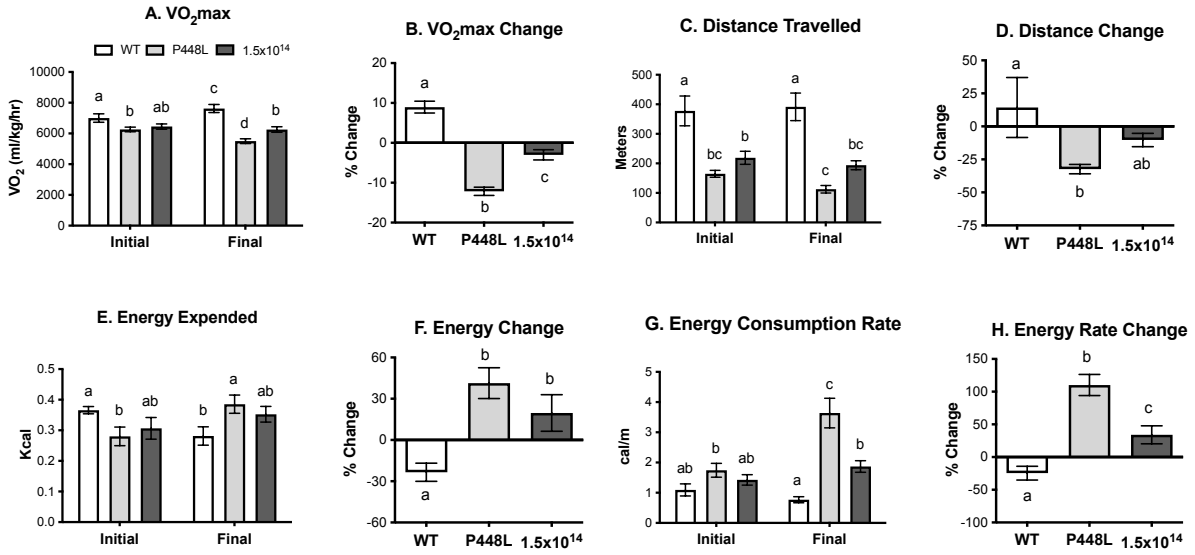

Figure 2.3: Energetics of exercise performance. Wild-type and mutant mice were injected with saline (WT and P448L, respectively), the latter also with $1.5x10^{14}$ vg/kg. After 12 weeks, VO_2max tests were performed (initial) on all mice, which then trained twice a week for 4 weeks followed by a final VO_2max test. **A & B,** VO_2max values for each time point and the change from initial to final. **C & D,** Distance traveled before mice fatigued, failing to reengage the treadmill, and the change from initial to final. **E & F,** The total energy expended during tests was calculated using indirect calorimetry and was normalized to the total distance traveled for each mouse in order to quantify energy consumption rate (**G & H**). Significant differences are represented by different letters, shared letters indicate no difference. WT, wild type; P448L, untreated. (n=5-6)

By contrast, training exacerbated the dystrophic phenotype in untreated $FKRP^{P448L}$ mice as VO_2max was reduced by over 10%. This decline was prevented by A6.C8hF treatment, as the slight reduction in VO_2max between tests of treated $FKRP^{P448L}$ mice was not significant. Moreover, the degree of relative change between tests was highly significant among all three

groups (Fig. 2.3B), clearly indicating the effect of impact training and treatment. Changes in running distances and energy rates (Fig. 2.3D, F, & H) reflected a similar relationship as impact training improved, impaired, or had no effect on wild-type mice, untreated FKRP^{P448L}, and treated FKRP^{P448L} mice, respectively. These results collectively suggest that although high dose treatment with A6.C8hF may not restore exercise capacity to wild-type levels, it prevents the deleterious effects of impact training and improves striated muscle functional efficiency.

Both FKRP^{P448L} groups of mice ran shorter distances in the initial tests while expending similar calories (Fig. 2.3C & E). Although this resulted in higher energy-consumption rates, these differences were not significantly different from wild-type mice (Fig. 2.3G). The protective effect on exercise-induced impact was also reflected in energy consumption rates. In fact, all three groups were significantly different from one another in the final test, with untreated FKRP^{P448L} mice having the lowest VO_2max and highest energy consumption rate (Fig. 2.3A & G). Treated FKRP^{P448L} mice displayed values closer to those of wild-type animals. These data indicate that FKRP^{P448L} mice work harder to run shorter distances while consuming less oxygen. By contrast, treatment with A6.C8hF partially restored these metrics and thus, exercise capacity.

2.3.4 High dose A6.C8hF partly ameliorates the dystrophic respiratory pattern and endurance exercise capacity in FKRP^{P448L} mice. Several pathological markers for assessing exercise impact training have been developed for dystrophic mice.[46-49] In addition to histological metrics, these include several exercise-induced markers in FKRP^{P448L} mice such as variability in respiration (VO_2cv & RER), energy expended, and the accumulation of motivational shocks.[70] In 4 of the 6 training sessions, the VO_2cv values for untreated FKRP^{P448L} mice were higher than those for wild-type mice while the treated FKRP^{P448L} animals displayed values that were either

significantly lower than the untreated mice or not different from wild-type mice (Fig 2.4A). A similar pattern was observed when comparing the overall differences between groups, which were highly significant, and when assessing differences in maximal RER values (Fig. 2.4B).

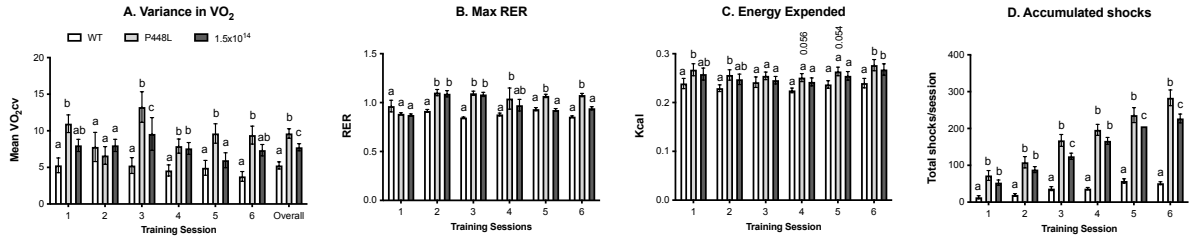

Figure 2.4: The effects of exercise impact training in the high-dose experiment. After an initial VO_2max test, wild-type mice and $FKRP^{P448L}$ mice were injected with saline (P448L) or $1.5x10^{14}$ vg/kg A6.C8hF then trained on respiratory treadmills twice a week for 6 sessions. Mice ran with sub-maximal effort, at the same speed and for the same time while respiratory gas exchange was continuously monitored. **A,** The fluctuating breathing pattern common to dystrophic mice was quantified by calculating the VO_2 coefficient of variation. **B,** Differences in maximum respiratory exchange ratios (RER) with each session. **C,** Total energy expended during each session was calculated using indirect calorimetry. **D,** Electrical shocks were used to encourage mice to reengage the treadmill and their quantification is a metric of motivation. In each panel, the numbers on the x-axis represent specific training sessions and different letters above the histograms are used to signify significant differences between any two means ($p<0.05$ unless otherwise indicated), shared letters indicate no difference. WT, wild type; P448L, untreated. (n=5-6)

No differences between groups were noted when assessing energy expenditure (data not shown) although by contrast, many differences were noted in the accumulation of motivational shocks (Fig. 2.4C). In fact, the number of shocks received by untreated $FKRP^{P448L}$ mice was approximately 6-fold higher than wild-type in all training sessions. However, treating $FKRP^{P448L}$ mice with A6.C8hF significantly reduced these numbers by the third session. Although levels were never restored to normal wild-type levels, they remained significantly below those of untreated $FKRP^{P448L}$ mice. Inordinate shock accumulation is a striking feature of $FKRP^{P448L}$ mice[49] that could be related to previously documented gait abnormalities.[71] Thus, these results suggest that A6.C8hF may partly restore many aspects of exercise performance that could be related to gait.

2.3.5 Mutant mice treated with A6.C8hF have decreased muscle degeneration, improved fiber size distribution, and decreased creatine kinase levels. After the final VO_2max test, all mice were sacrificed, and different muscles were collected. Compared to untreated FKRP^{P448L} mice, treated FKRP^{P448L} mice had larger skeletal muscle myofiber sizes with fewer centrally located myonuclei (Fig. 2.5A-E).

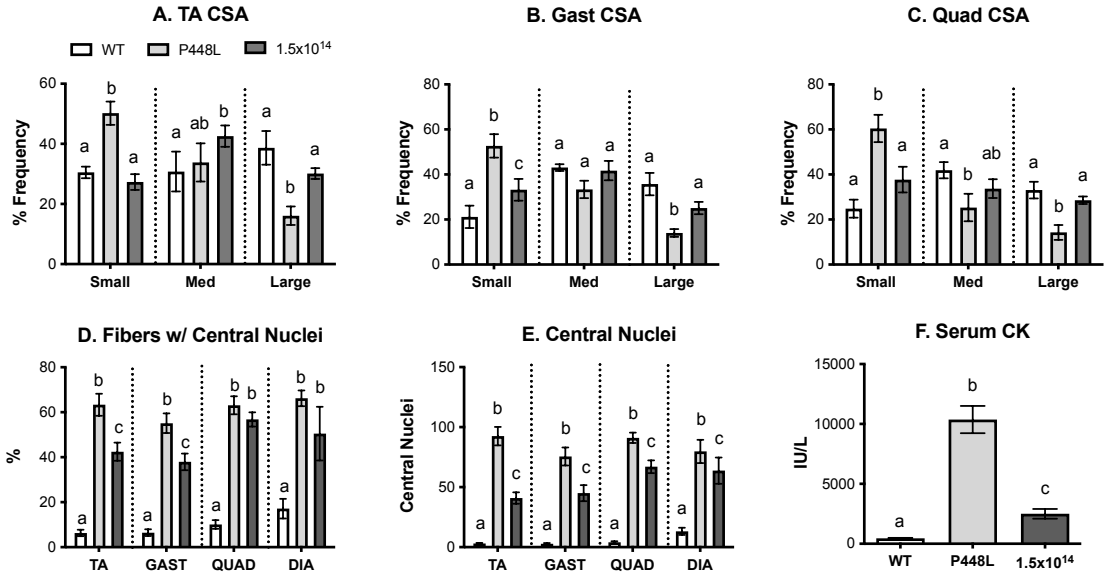

Figure 2.5: Morphological changes induced by *FKRP* delivery. 8-month-old FKRP^{P448L} mice were treated systemically with $1.5x10^{14}$ vg/kg A6.C8hF and analyzed 4 months later. **A-C,** Fiber cross-sectional area (CSA) of the indicated muscles parsed by fiber size groups: <3000 μm small, 3001-7000 μm medium and >7000 μm large. **D & E,** Fiber and nuclei counts per field in different skeletal muscles (TA, tibialis anterior; GAST, gastrocnemius; QUAD quadriceps; DIA, diaphragm). **F**, Serum creatine kinase levels in treated mice. Significant differences are represented by different letters, shared letter indicates no difference. WT, wild type; P448L, untreated. (n=3-5)

This was generally true for all muscles tested, although the diaphragm displayed the smallest changes between treated and untreated mice. The most dramatic response to treatment was the near 5-fold reduction in serum creatine kinase levels in treated vs. untreated mice (Fig. 2.5F).

These data together suggest that A6.C8hF reduces exercise-induced muscle damage that activates cycles of necrosis and regeneration that lead to skeletal muscle atrophy.

2.3.6 AAV injection leads to non-uniform FKRP expression in wild-type and treated FKRP^{P448L} mice. We performed immunofluorescence (IF) analysis of FKRP localization in muscle cryosections using Ab607. We first examined the tibialis anterior and heart from mutant mice treated with $4x10^{11}$ vg/kg A6.C8hF at 10 weeks post-injection (Fig 2.6A).

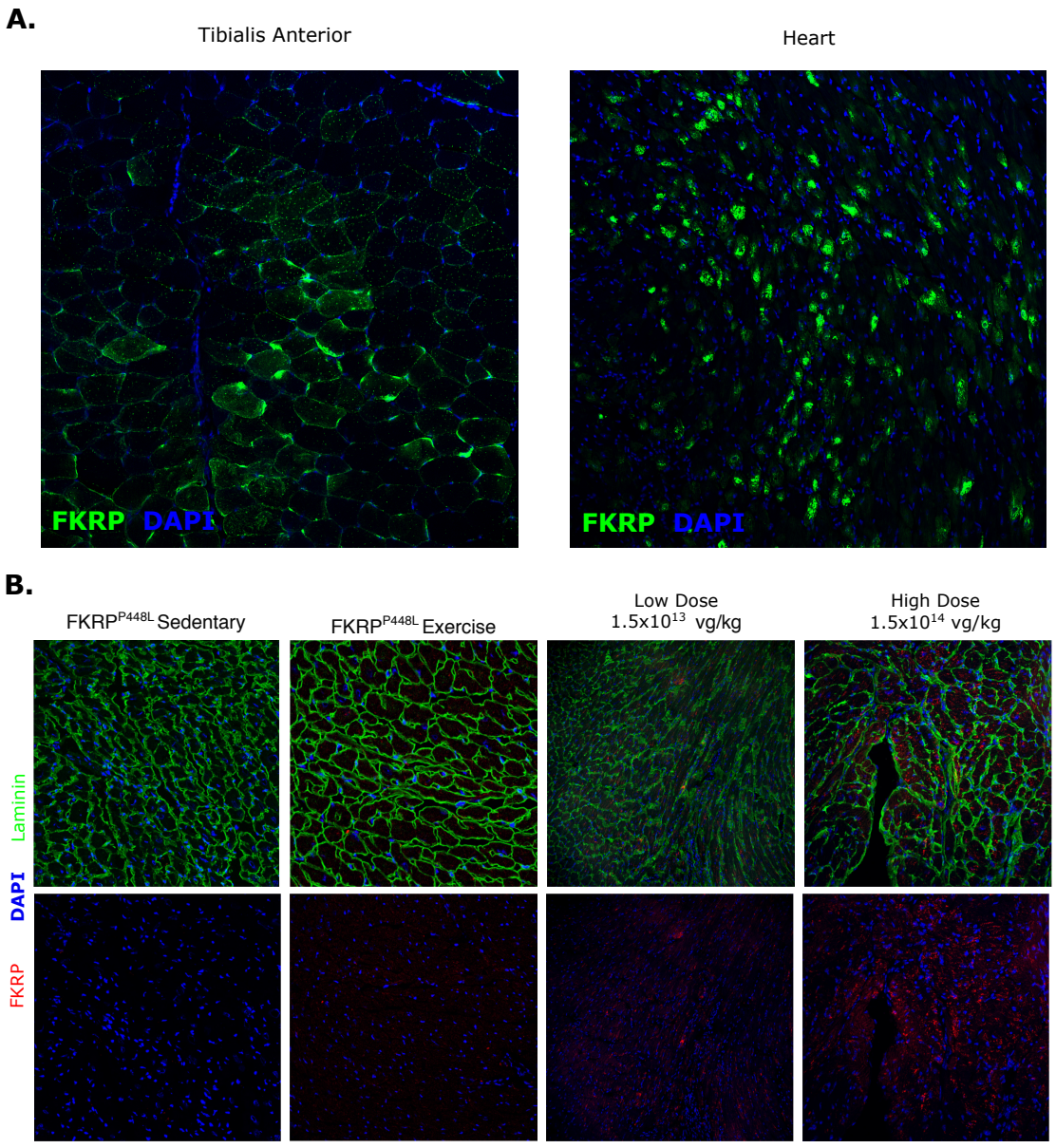

Figure 2.6: Immunofluorescent staining reveals mosaic expression of exogenous FKRP. A, TA and heart muscles from FKRP^{P448L} mice treated with 4x10^{11} vg/kg of A6.C8hF were isolated 10 weeks post injection and cryosections were prepared and analyzed. Shown is immunostaining for FKRP (green); DAPI staining is shown in blue. **B,** Cryosections from hearts of FKRP^{P448L} mutant mice comparing FKRP expression in untreated mice following no exercise (sedentary, left-most panels), and in untreated mice (active) and treated mice that were exercised, all at 16 weeks post-injection. Treated mice received an intravenous injection with a high (1.5x10^{14} vg/kg) or low (1.5x10^{13} vg/kg) dose of A6.C8hF and were exercised. Shown is immunostaining for FKRP (red) and Laminin (green); DAPI staining is shown in blue.

At this timepoint, FKRP was widely expressed in both muscle types, albeit in a mosaic pattern, consistent with previously reported results.[22] Although clearly detectable levels of FKRP were not observed in every myofiber (Fig. 2.6A), the grip strength and treadmill data suggest that there was sufficient FKRP expression to partially rescue the disease phenotype (Fig. 2.2-2.5). While endogenous FKRP was difficult to detect in untreated mice, more FKRP immunofluorescence was observed in heart tissue from exercised vs sedentary mice (Fig. 2.6B and not shown). In contrast, treated (sedentary) mice displayed robust expression of FKRP in a dose-dependent manner. The effect of exercise is intriguing, as while it has previously been shown that $FKRP^{P448L}$ mutations can lead to a cardiac phenotype,[34] to our knowledge, exercise-induced FKRP expression has not been previously studied.

2.3.7 Wild-type animals treated with AAV-FKRP vectors displayed normal muscle physiology. To explore other avenues of delivering FKRP to skeletal muscles, we performed additional assays in wild-type mice injected with vectors made with AAV6, AAV9 or AAVMYO1 capsids. These studies also provided a way to examine the effects of exogenous FKRP in muscle already expressing normal levels of the enzyme. One previous report suggested that overexpression of FKRP could impair the formation of a functional DGC.[32] Our studies used AAV6, as above, but also 2 additional vector types. Gene therapeutics featuring AAV9 capsids are commonly used in clinical trials for different neuromuscular disorders,[72] while the recently developed AAVMYO1 was reported to provide enhanced muscle transduction.[53]

The first study consisted of wild-type mice injected with A6.C8hF at doses of $4x10^{13}$, $2x10^{14}$, or $4x10^{14}$ vg/kg to determine whether this vector caused an increase in susceptibility of muscles to contraction-induced injury. These high doses were a used in this preliminary safety

assessment, as doses at or exceeding $1x10^{14}$ vg/kg have often led to serious adverse events in patients with various neuromuscular disorders.[50, 51, 73, 74] This is important because a high dose AAV-mediated FKRP therapeutic, plus endogenous FKRP, provides the ability to maximize potential expression. Some of these mice underwent gastrocnemius muscle physiology assays 5 weeks later and others were tested at 10 weeks. However, we did not observe any deleterious impact on mechanical properties at these doses (Supplemental Fig. 2.1).

Finally, the AAV9 and AAVMYO1 vectors were injected into wild-type mice at doses of $6.4x10^{12}$, $2x10^{13}$, and $6.4x10^{13}$ vg/kg. The latter two cohort of mice were analyzed for a variety of properties at 4-, 6-, 8-, 10-, 12-, and 14- weeks post-injection to evaluate effects on muscle physiology (Fig 2.7). At 6-, 10-, and 14- weeks post-injection, fatigue assays were performed in which mice ran on a treadmill at a speed of 10 meter/sec for 5 minutes and 1 meter/sec/min increases until fatigue was reached (Fig. 2.7A-C). No differences were detected between groups at each time point. Moreover, the absence of differences in relative change within and between groups similarly demonstrates an absence of detrimental effects on running fitness and fatiguability following vector delivery. We also examined forelimb grip strength between 4-, 8-, and 12- weeks post-injection. Although mice treated with AAV9 displayed reduced force over time, there were no differences between groups at any time point. In fact, all the mice (treated and untreated) experienced a decrease in strength between 10- and 14-weeks post-injection groups, which typically occurs when mice habituate to the grip-strength assay.

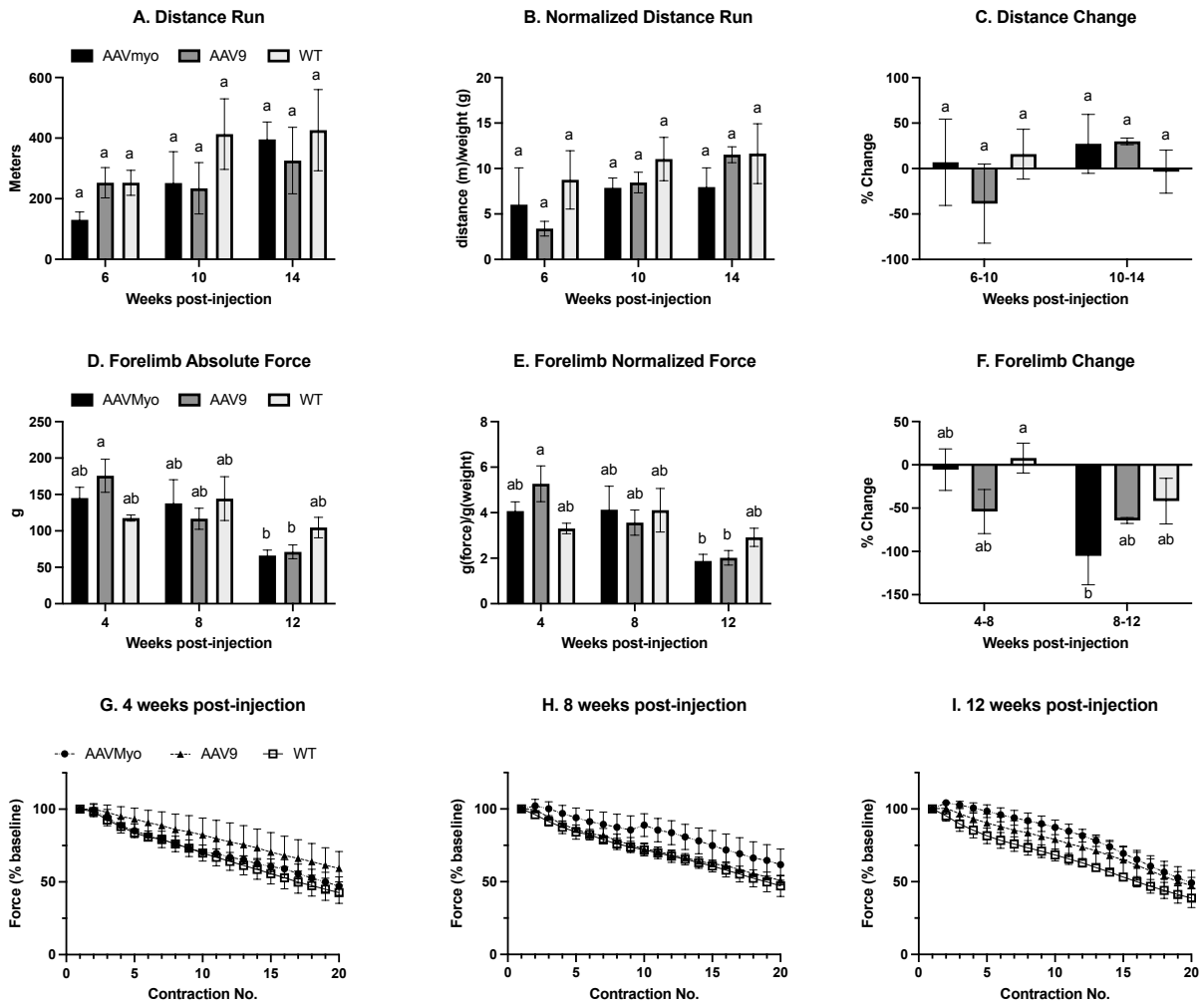

Figure 2.7: Whole-body and isolated limb physiology of wild-type mice treated with AAV-hFKRP. A, Distance run by mice on a treadmill by mice injected with either saline (WT) or $6.4x10^{13}$ vg/kg of A9.C8hF or AM.C8hF. **B,** Distance run normalized to mouse weight. **C,** Percent distance changed relative to previous absolute distance measured. **D,** Forelimb grip strength. **E,** Forelimb grip strength normalized to mouse weight. **F,** Percent forelimb grip strength changed relative to absolute grip strength. **G-I,** Repeated cycles of plantarflexion eccentric contraction induced injury (20x) in the right hind limb of mice at 4-, 8-, and 12-weeks post-injection measured by hindlimb torque. Limb was stimulated with 10mA at a frequency of 100Hz for 0.4 seconds with a 9 second rest interval between contractions. Significant differences are represented by different letters, shared letter indicate no difference. WT, untreated. (n=3-4)

Another commonly used assay in mouse muscle analysis is the ankle plantarflexion assay, in which ankle torque over 20 eccentric contractions is quantified using a high yet physiologically relevant stimulation frequency that elicits a maximal response. The assay is designed to assess

force generation in addition to fatigue caused by repeated eccentric contractions. At all timepoints, torque declined to 50% of starting baseline measurements, consistent with contraction-induced fatigue (Fig. 2.7G-H). However, no differences were detected between any of the three groups at any timepoint. This includes potential differences in torque at a given contraction as well as the relative change from baseline. These results further suggest that A9.C8hF and AM.C8hF treatments at a dose of $6.4x10^{13}$ vg/kg did not compromise muscle force generation or enhance fatiguability.

To identify potential adverse consequences of exogenous FKRP expression in cardiac and diaphragm muscles, we used ultrasound imaging to measure cardiac ejection fraction and fractional shortening as well as diaphragm displacement. Ejection fraction measures the percent of blood leaving the left ventricle, while fractional shortening is a measure of the heart's contractility; both of which are common indicators of cardiac function. Diaphragm displacement is likewise an indicator of respiratory function. No differences were detected between untreated and treated groups (Fig. 2.8A-C).

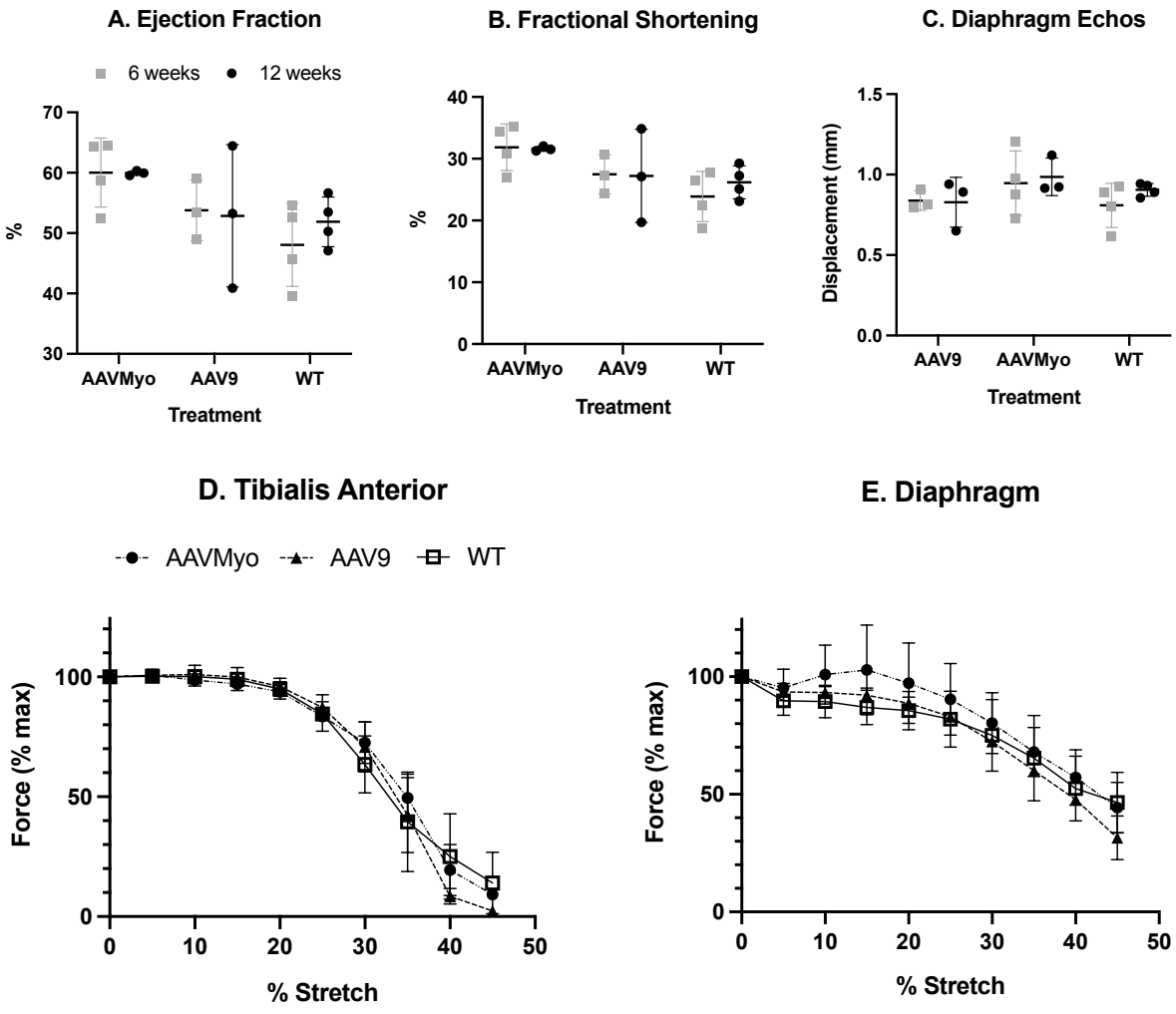

Figure 2.8: Cardiac hemodynamics and skeletal muscle mechanics following AAV delivery to wild-type mice. Mice were untreated or injected with $6.4x10^{13}$ vg/kg A9.C8hF or AM.C8hF. **A-C,** Ultrasound imaging of heart and diaphragm function at 6- and 12-weeks post-injection. **D & E,** Force:length relationship of TA and diaphragm muscles from same mice at 18 weeks post-injection. Muscles are stretched end-to-end and optimal length is determined at maximum isomeric twitch force (see Methods). No differences were detected in these data. WT, untreated. (n=3-4)

At the experimental endpoint (18 weeks post-injection), skeletal muscle function was further assessed using a contraction-induced injury protocol on tibialis anterior and diaphragm muscles. Here, muscles were stretched by an additional 5% between contractions to measure specific force development and to examine the effects of contraction-induced injury on force. As

with the other functional assays, no differences were detected between treated and untreated groups (Fig 2.8D & E). These data complement those from previous tests, which together reveal no adverse consequences from exogenous FKRP overexpression in skeletal or cardiac muscles using the assays shown (Fig. 2.7 & 2.8).

2.4 DISCUSSION:

This study demonstrated that A6.C8hF (carrying the *FKRP* cDNA lacking UTRs) ameliorated pathophysiology associated with the dystrophic phenotype in aged $FKRP^{P448L}$ mice. Moreover, it also significantly minimized exercise-induced impacts on skeletal muscle structure and function, with a treatment benefit proportional to the dose of A6.C8hF administered and without obvious safety side effects. One focus of our investigation was to develop a transgene with high expression levels in striated muscles. Use of such a transgene can enable studies of safety while also facilitating therapeutic expression levels at lower vector doses. It should be noted that safety and toxicity concerns have been growing in the field, with adverse events from either the vector or transgene being observed in a variety of high dose, neuromuscular disease AAV trials.[72, 75]

RNA G-quadruplexes (RGQ) are known to regulate gene expression and have been targeted as a strategy to ameliorate or worsen genetic disease pathologies.[59, 76] We discovered that complete removal of both the 5' and 3' UTRs led to increased gene expression (Fig. 2.1). These data suggest the presence of inhibitory regulatory sequences within the UTRs of *FKRP*, which could provide a potential target for fine-tuning gene expression. The occurrence of toxicity associated with gene overexpression has sometimes been resolved by targeting UTRs,[56, 77] which continue to be evolved for even more influence over protein production.[78]

Differences in the design of the various experiments in our study prevent direct comparisons of many metrics. Nevertheless, we can compare several differences between treated and untreated FKRP^{P448L} mice within individual experiments to gauge the relative sensitivity to gene delivery. Overall, treatment had a clear beneficial effect, and no adverse events were observed at any doses in either wild-type or mutant mice. It should be noted that while improvement occurred in a dose-dependent manner, none of the functional metrics were restored to wild-type levels using the doses tested. This was not unexpected, as FKRP mutations in both animal models and patients leads to a degenerative disease that progressively develops and worsens with age,[79-81] compounding challenges to drug efficacy. Higher doses or ancillary treatments to enhance muscle mass and strength may be needed when degeneration is advanced.

Other FKRP gene therapy studies generally used young FKRP^{P448L} mice and reported many significant improvements in the structure and function of skeletal and cardiac muscle.[30, 34] Only one study used an exercise paradigm to assess therapeutic efficacy in FKRP^{P448L} mice.[37] While that study did not incorporate respiratory measures or impact training, a variety of age groups were tested, including aged 39-week-old mice treated for 12 weeks. Those treated FKRP^{P448L} mice displayed increased fatigue resistance, running time and maximal speed in all age groups, although the differences reported were not statistically significant. Regardless, that trend is consistent with the current study and further suggests that systemic FKRP gene therapy can enhance exercise capacity even in aged FKRP^{P448L} mice.

Demonstrating that our therapeutic can improve exercise capacity is especially meaningful, as the metrics measured are largely dependent upon cardiac rather than skeletal muscle function. Thus, the improved performance in VO_2max tests suggests that cardiac function is specifically enhanced (Fig. 2.3). These results are complemented by others,[35] which demonstrate that *FKRP*

delivery to mutant mice can improve some aspects of cardiac contractility in stress tests. Left ventricle dysfunction has been described in FKRP^{P448L} mice[70] and often occurs in human subjects with LGMDR9. Moreover, cardiac and respiratory impairment directly contribute to mortality in many individuals with different FKRP mutations and are predictors of long-term survival. It is not unreasonable, therefore, to presume that systemic FKRP gene therapy could ameliorate the primary cause of mortality in LGMDR9 patients.

Our AAV vector also protected FKRP^{P448L} mice from many degenerative effects of impact training. This included changes to muscle structure, serum creatine kinase levels and exercise capacity (Fig. 2.5). Impact training is known to accelerate and exacerbate muscle degeneration in dystrophic mice and is considered an advanced stressor.[82] The fact that A6.C8hF protected aged FKRP^{P448L} mice from impact training is significant and suggests that treatment overcame both the accumulated effects of age, as indicated by improved functional metrics before initiating training, as well as the damage from repeated exercise, as indicated by the improved functional metrics during the training sessions and by the histological metrics. Differences in cross-sectional area and central nucleation, between treated and untreated FKRP^{P448L} mice, were more apparent in TA and quadriceps muscles than in the gastrocnemius or diaphragm. The former two muscles have a higher type II fiber composition than the latter mixed-fiber type muscles. This result suggests that FKRP gene therapy may be especially effective in stabilizing predominantly fast twitch muscles that are more affected in different muscular dystrophies.[83, 84]

Safety assessment with exogenous FKRP expression

While studies here and by others show improved phenotypic outcome from AAV-FKRP delivery, we also explored the effects in wild-type mice to monitor potential adverse events from exogenous

FKRP expression above normal muscle expression. These exogenous expression levels were augmented using a strong, muscle-specific regulatory cassette (CK8e), the removal of UTRs from the *FKRP* cDNA and the use of myotropic AAV capsids, especially AAVMYO1. Three doses of $4x10^{13}$, $2x10^{14}$, and $4x10^{14}$ vg/kg of A6.C8hF indicated that treated wild-type mice continued to gain strength, did not fatigue more rapidly, and showed no detrimental effects on mechanical properties (Supplemental Fig. 2.1). We also performed a longer study with wild-type mice untreated or injected with A9.C8hF and AM.C8hF. These groups of mice showed no significant differences in distance run, forelimb grip strength, or TA, diaphragm muscle or hind limb eccentric contraction induced fatigue over time, nor were these measurements significantly different between groups (Fig. 2.7). In these studies, treated and untreated mice also showed no change in ejection fraction, fractional shortening, nor diaphragm displacement over time (Fig. 2.8). Overall our data support the safety of A6.Ch8F, A9.C8hF, and AM.Ch8F as gene therapies for LGMDR9, as our assays show that none of these treatments led to adverse effects on wild-type mouse physiology. These results demonstrate that expression from the vectors used was not deleterious to muscle function and was able to ameliorate disease pathology in mutant mice.

Conclusions and future directions

Our studies further support the feasibility of gene therapy for disorders resulting from FKRP mutations. Like previous studies, we observed an overall significant amelioration of disease phenotype in adult $FKRP^{P448L}$ mice.[30, 31, 37] Further, we did not observe any obvious detrimental effects from expression of FKRP using a variety of AAV vectors at different doses in wild-type mice. A potential G-quadruplex in the 5' UTR may serve to limit expression, although we did not dissect individual bases in the 5' or 3' UTRs of the *FKRP* mRNA that mediate this effect. The

difficulty encountered by many labs in detecting endogenous *FKRP* expression suggests that extremely low levels of the enzyme is all that is needed for normal glycosylation of a-DG. It is possible that inhibitory UTR sequences may serve a role in limiting overexpression during normal muscle activity, although further studies would be needed to clarify this issue. Importantly, the safety of this therapeutic observed in our studies supports continued advancement of methods for gene therapy to treat patients carrying mutations in the *FKRP* gene.

2.5 MATERIALS & METHODS:

Animals

All animal experiments were approved by the Institutional Animal Care and Use Committee of the University of Washington or Washington State University. For the $FKRP^{P448L}$ mutant experiments, mice were obtained from the Lu lab,[34] and maintained by the Rodgers Lab at Washington State University. The studies using $FKRP^{P448L}$ mice began when the mice were 10 months old. The other mouse studies were performed in C57BL6 wild-type male mice aged 6-35 weeks at age of injection.

Plasmid construction and vector production

The coding region of mouse *Fkrp* was PCR amplified (Forward primer: 5' TTGTTAACATGCGGCTCACCC 3'; Reverse primer: 5' TACCGGTTCAACCGCCTGTC 3') from mouse muscle cDNA. The resulting DNA fragment was digested with *Hpa*I and *Age*I and ligated into an AAV backbone vector containing a muscle specific CK8e promoter and synthetic

poly A tail, as previously described.[60] Briefly, a custom AAV transfer plasmid containing the previously described muscle-specific CK8e regulator cassette[3, 60-65], a 1,482 bp cDNA expression construct for native mouse *Fkrp* mRNA (NCBI CCDS20853.1), a synthetic polyA signal[60] and flanking AAV serotype 2 inverted terminal repeats was constructed using standard recombinant methodology. The resulting plasmid, pAAV-CK8e-FKRP, was then used to co-transfect HEK293 cells along with the pDGM6 helper plasmid to generate AAV6 vector as previously described.[85] For AAV9 (pA9.C8hF) and AAVMYO1 (AM.C8hF) vectors the human *FKRP* cDNA was PCR amplified and cloned into pAAV-Ck8e-FKRP in place of the mouse cDNA. These latter vector preparations were produced and purified by Forge Biologics (Grove City, OH).

Antibody production and purification

Rabbit polyclonal antisera was generated against a peptide near the C-terminus of the FKRP sequence that was identical in the mouse and human proteins (as a fusion with KLH: KLH-C-APNNYRRFLELKFGPGVIENPQYPNP) by Covance (Denver, PA). Affinity purification was performed using a maltose-binding protein fusion of the antigenic peptide on a MBPTrap HP columns (GE Healthcare) and coupled to Ultralink Biosupport polyacrylamide resin (Thermo Scientific) as per manufacturer's instructions. The FKRP-C antibody (named Ab607) was affinity purified by HPLC through MBP-FKRP coupled beads and stored in BSA and NaN_3.

Cell culture

Mouse C2C12 cells were plated at ~80% confluence on gelatin-coated 6-well plates with standard growth media (DMEM, 20% FBS, 1% penicillin-streptomycin) overnight, then washed three times with 1x Saline G prior to infection with rAAV6-CK8-mFKRP. Vectors were diluted to the desired concentrations in differentiation media (DMEM, 2% HS, 1% Penicillin-Streptomycin). Cells in each well were incubated with 0.5 ml of diluted virus at 37ºC for ~ 2 hours and brought to a final volume of 2 ml with differentiation media and incubated overnight prior to refeeding with fresh differentiation media. Western analysis was performed at day 3 post-differentiation to determine FKRP expression.

Gene delivery

Mice were randomly assigned to groups prior to treatment. They were then anesthetized by an intraperitoneal injection of 0.25 mg/g 2,2,2-tribromoethanol or isoflurane and subsequently injected retro-orbitally (RO) (150 µl at doses of $1.5x10^{13}$, $4x10^{13}$, $1.5x10^{14}$, $2x10^{14}$, or $4x10^{14}$ vg/kg), intramuscularly (30 µl at doses of $1x10^{10}$ vg and $1x10^{11}$ vg), or intravenously via the tail vein (150 µl at doses of $6.4x10^{13}$ vg/kg).

Western analysis

Frozen muscles were ground to fine powder and proteins extracted in 1x Laemmli buffer (62.5 mM Tris-HCl, pH 6.8, 2% SDS, 10% glycerol, protease inhibitor (Roche)). Lysates were centrifuged at 10,000x g for 10 min at 4ºC, and supernatants transferred to fresh tubes. Total

protein concentration was determined by BCA Assay (Pierce). Prior to loading, 50 mM DTT and 0.01% bromophenol blue were added to samples and heated at 94ºC for 4 min. For each sample, 20 μg of total protein was separated on 4-12% SDS-PAGE (Life Technologies), transferred to PVDF membranes (GE Healthcare), and blocked (5% skim milk, 1x PBS, 0.1% Tween-20) for 1hr at room temperature. Blots were probed with Ab607 (1:2000) overnight at 4ºC, washed in 1x PBS-Tween, incubated with HRP-Rabbit secondary (1:20,000, Pierce) and developed with ECL chemiluminescent reagents (GE Healthcare).

Physiology

Grip Strength. Fore- and hindlimb grip strength of mutant mice and controls were measured using the Columbus Instruments Grip Strength Meter (Columbus, OH). Forelimb assays used the T-bar or the wire mesh attachment, while hindlimb assays used only the wire mesh attachment. For each mouse, measurements were replicated 5 times in each session with at least 1 min rest between measurements as this ensures accuracy, reduces variability, and prevents habituation. Means were then calculated for each mouse at each time point and these values were then used to create means for each group.

Treadmill Acclimation & Forced Exercise Protocol Design for Mutant Mice. We utilized a four-lane Oxymax FAST Modular Treadmill System equipped with shock monitors (Columbus Instruments, Columbus, OH) to measure exercise capacity and respiration during forced exercise of the mutant mice. The motivational shock units were set at level 2.5, providing 0.65 mA of constant current for 200 ms at a frequency of 1 Hz, and fresh air was pumped into the treadmill chamber at a rate of 0.6 L/min. Acclimation runs were performed by placing mice on stationary

treadmills for 5 minutes with the shock unit engaged. The treadmill was then set at a speed of 5 m/min and mice walked for 5 additional min. This process was repeated for three consecutive days or until mice received 3 or fewer shocks while walking. Exercise training is an excellent means to assess disease pathophysiology in dystrophic mice and is often used to exacerbate the dystrophic phenotype.[46-49] Mutant mice injected with the high dose were trained on a treadmill to assess exercise-induced impact on the dystrophic phenotype. Initial VO_2max tests were performed on high dose mice 3 months post injection and were followed by 6 training sessions over a month, 2 sessions/week, and then a final VO_2max test. This protocol was recently customized for $FKRP^{P448L}$ mice[49] and is similar to a protocol we previously established for mdx mice.[48] Briefly, VO_2max tests began with mice acclimating on a stationary treadmill for 5 min. Treadmill speed then increased at rates of 5, 9, 12 and 15 m/min for 5 min at each speed. The speed was then increased 1.8 m/min every 2 min until mice reached exhaustion, as indicated by their failure to reengage the treadmill for 10 sec, after which the shock units were turned off. A VO_2max value for each mouse was identified by a rapid increase in the respiratory exchange ratio (RER) approaching 1.1 in combination with a peak VO_2 (ml/kg/hr) and caloric expenditure was calculated using indirect calorimetry as described.[48, 86, 87] Mice trained on a 0^o incline that began with a 5 min stationary phase followed by 2 min at 5 m/min, 8 min at 8 m/min and finally 25 min at 12 m/min.

Muscle Histology and Serum Creatine Kinase Assays. Tibialis anterior, gastrocnemius, quadriceps and diaphragm skeletal muscles as well as the heart were collected from mutant mice and flash frozen in -140^{o}C isopentane. Skeletal muscles were then sectioned at 10 μm on a cryostat, fixed for 10 minutes in 4% paraformaldehyde and stained using hematoxylin and eosin.

Each slide contained 8-10 sections based on muscle size and stained slides were imaged using a Nikon Eclipse Ti and a 20X lens. At least 5 images were collected for each individual muscle. Histological analyses were performed using Adobe Photoshop (Adobe, San Jose, CA) to count all muscle fibers and all muscle cell nuclei in each image, while cross sectional area was determined using ImageJ (NIH, Bethesda, MD). To measure serum creatine kinase, blood was removed via cardiac puncture and serum was collected by centrifugation at 10,000 rpm for 10 min. The colorimetric Serum Creatine Kinase Assay Kit (Abcam, Cambridge, MA) was then used with a spectrophotometer to record enzymatic activity following the manufacturer's instructions.

Gastrocnemius Force. Supplemental Figure 2.1. Muscle physiology was performed as previously described for wild-type gastrocnemius muscles.[88] Wild-type mice treated retro-orbitally with high doses of A6.C8hF were examined 5 and 10 weeks post-treatment. Untreated, age matched mice were also examined as controls.

Treadmill Fatigue Analysis for wild-type mice. Wild-type mice were acclimated to the treadmill (motorized Exer-3/6 shocker for mice and rats, Columbus instruments, Columbus, OH, USA)) for 5 min at 10 m/s before each run. The speed was then increased at 1 m/s every minute until voluntary stoppage. Stoppage is measured as the time at which a mouse reacts to grid five times or spends a maximum 5 s sitting on the electrical grid at setting (0.7 mA, 200 ms/shock). This test was performed at 6, 10, and 14 weeks post-injection.

Ankle Torque Plantar Flexion. Wild-type mice were anesthetized with isoflurane and the lower right hind limb was shaved. Mice were placed on a heated platform (37°C) and the foot of the mouse was attached to the lever of the servomotor (Aurora Scientific, model 305) with the ankle joint at a 90° angle. Needle electrodes were inserted near the sciatic and into the quadriceps of the right hind limb to be stimulated at 10 mA. After initial measurements of maximum isometric twitch force and point of maximum tension were recorded, we performed a protocol consisting of 20 eccentric contractions at 100 Hz. The muscles were stimulated for 0.4 seconds per contraction, with 9 second rest intervals between measurements. The signal output of the force transducer is displayed on a storage oscilloscope (Tektronix Model 5111) coupled to a microcomputer used for data acquisition and storage. This test was performed on mice treated mice with A9.C8hF or AM.C8hF at 4, 8, and 12 weeks post-injection.

Ultrasonography. Echocardiograms were performed on wild-type mice by the University of Washington Center for Translational Muscle Research core. Echocardiography was conducted with Vevo 3100 high-frequency, high-resolution digital imaging system (VisualSonics). The mice were slightly anaesthetized with 1-1.5% isoflurane in oxygen. The parasternal short axis view at the mid papillary level was used to obtain M-mode images for analysis of fractional shortening, ejection fraction, and other cardiac functional parameters. Diastolic function was assessed by measurement of trans mitral flow parameters from apical 4-chamber view with pulsed wave Doppler. Tissue Doppler imaging was performed by placing sample volume at the septal corner of the mitral annulus. Mice were anesthetized by isoflurane and taped to a warmed platform (37C). This test was performed at 6 and 12 weeks post injection.

Tibialis Anterior Force Frequency. Prior to operative procedures, wild-type animals were anesthetized with isoflurane in an induction chamber and were maintained under anesthesia using a nose cone during the procedure. A small incision to expose the distal tendon of the TA muscle was made. The intact tendon was tied to the lever arm of a servomotor (Model 305-B, Aurora Scientific, Richmond Hill, ON, Canada). The hind-limb was stabilized by pinning the knee and securing the foot to a heated platform (37°C). Needle electrodes are inserted on either side of the sciatic nerve. Stimulation voltage and muscle length were adjusted for maximum isomeric twitch force and the optimal TA length was determined (L_0). Tetanic twitch force was then measured at increasing stretch of L_0: 0%, 5%, 10%, 15%, 20%, 25%, 30%, 35%, 40%, and 45%. The signal output of the force transducer is displayed on a storage oscilloscope (Tektronix Model 5111) coupled to a microcomputer used for data acquisition and storage. Following the measurements of power, the muscle is isolated and removed from the animal. The anesthetized animals were euthanized, and tissues were collected for histology and analysis.

Diaphragm Force Frequency. The diaphragm strip measurement begins with whole tissue removal while mouse is under anesthesia. In a dissection bath (136.5mM NaCl, 5mM KCl, 1.8mM $CaCl_2$ 0.5mM $MgCl_2$, 0.4mM NaH_2PO_4, and 11.9mM $NaHCO_3$), sutures are tied around both ends of a small strip cut along the myofibers of the diaphragm. The strip was placed in a bath (121mM NaCl, 5mM KCl, 1.8mM $CaCl_2$ 0.5mM $MgCl_2$, 0.4mM NaH_2PO_4, 24mM $NaHCO_3$, and 5.5mM glucose) and the sutures were tied to the servomotor (Model 300-C, Aurora Scientific, Richmond BC, Canada) and force transducer. A similar procedure to the TA muscle strength assay above was used, with the stimulation voltage and then muscle length adjusted for maximum isomeric twitch force and the TA length is measured (L_0). Tetanus (point

at which maximum tension is generated) was measured at increasing stretch of L_0: 0%, 5%, 10%, 15%, 20%, 25%, 30%, 35%, 40%, and 45%. The signal output of the force transducer is displayed on a storage oscilloscope (Tektronix Model 5111) coupled to a microcomputer used for data acquisition and storage.

Tissue collection and Immunohistochemistry

At termination of the mice, the tibialis anterior, soleus, gastrocnemius, diaphragm, heart, liver, and spleen were all collected. Half of each muscle was positioned on OTC Compound embedding medium for cryo-sectioning while the other half plus the bilateral muscle of limbs were flash frozen in liquid nitrogen. Previously characterized mouse FKRP antiserum was used to visualize FKRP overexpression in cardiac and skeletal muscle cryosections.[3] Transverse and longitudinal 10-μm muscle sections were blocked in AffiniPure Fab fragment goat anti-mouse IgG (1:25 dilution; Jackson ImmunoResearch) diluted in 2% BSA for 1 hr to prevent cross-reaction with endogenous mouse antibodies. Samples were washed in 1x PBS and incubated in primary antibodies at room temperature for 2 hr. In addition to incubating with FKRP-C (1:200), samples were co-stained with organelle markers (BD Biosciences); GM130 (1:500), BiP/GRP78 (1:200), Bcl-2 (1:200), EEA1 (1:250). Sections were washed in 1x PBS and re-blocked in 2% BSA for 10 min prior to secondary incubation with Alexa Fluor 488 goat anti-rabbit IgG (1:500; Molecular Probes) and Alexa Fluor 594 goat anti-mouse IgG1 or IgG2A (1:200; Molecular Probes). Samples were washed with 1x PBS prior to mounting with Fluoromount G (Southern Biotech).

Statistical Analysis

Data are presented as means ± SEM and statistical comparisons were made using Prism (GraphPad Software, La Jolla, CA). Significant differences ($p \leq 0.05$ unless otherwise noted) were determined using a Student's t-test or with a 1- or 2-way analysis of variance coupled to Tukey's post-hoc test for multiple mean comparisons. Significant differences are represented by different letters and a shared letter indicates no difference. For example, three data points labeled a, ab, and b represent a significant difference between a and b, as different letters indicate significance. There is no difference between a and ab or ab and b, as they share letters.

CHAPTER 3: *In Vivo* Assessment of Synthetic Self-Assembling Nucleocapsids for Targeted Therapeutic Delivery

This work was performed in collaboration with Audrey Olshefsky of the King and Pun groups at the University of Washington

3.1 ABSTRACT:

Improving targeted therapeutic delivery is crucial for the development of precision medicine, which is the next great step forward in patient treatment and safety. Using a high-throughput synthetic nucleocapsid system, we evolved a library of surface mutations and miniprotein binders to identify characteristics that enhance tissue tropism. After two steps of selection *in vivo* we obtained nucleocapsid constructs enriched in the heart, skeletal muscle, and T41 tumors. We not only demonstrated the increased targeting to specific tissues but also depletion of constructs that reached the liver, spleen, and other major organs. These data represent a comprehensive evaluation of synthetic nanoparticles evolved and ultimately tailored to the delivery of specific therapeutics.

3.2 INTRODUCTION:

The tissue-targeting and safety of therapeutic delivery systems remains one of the greatest barriers within the field of gene therapy. As previously mentioned, AAVs are the most used system for muscle gene therapies, and only a few have been approved by the FDA for clinical use. However, few AAVs are specific to a single tissue, some tissues such as muscle require high doses to achieve transduction. Unfortunately, these high doses of clinical AAV therapeutics (≥ $2x10^{14}$vg/kg) have been associated with serious adverse events and patient deaths[50] due to liver

toxicity. While this problem is being addressed and continual improvements are being made to de-target the liver and other unnecessary organs, broadly neutralizing antibodies that recognize many AAV serotypes exist in a significant portion of the population.[89] The result of this is an innate immunity present in many patients that may otherwise be perfect candidates for AAV-mediated gene therapy. Patients in clinical trials are often put on immunosuppressants for the first few months of the treatment to avoid these risks, but these drugs also pose a significant danger as patients become more susceptible to infection. These and other obstacles necessitate the continued development of AAVs and other potential delivery systems.

One possible method in which to survey potential AAV components and AAV alternatives is via selection of a library of variants *in vivo*, in which millions of potential ligands can be screened simultaneously for desired properties.[90] This technique has been used in previous work to identify AAVs with improved tropism, such as the development of AAVMYO which is an AAV9 mutant that displays enhanced muscle delivery (including diaphragm and cardiac) and the *in vivo* assessment of AAVMYO to create AAVMYO2 and AAVMYO3.[52, 53] While the reason for this specificity, be it tissue-targeting or de-targeting, remains unknown, other evidence shows high-affinity ligands on the surface of AAVs increase cell-specificity.[91] To further explore this behavior, we decided to utilize a novel synthetic system previously engineered in the Institute of Protein Design at the University of Washington.[92] This system is comprised of synthetic proteins that bind and package their own mRNA genome to form a nucleocapsid, which can designed with desired traits. These have been termed "synthetic nucleocapsids" (synNC), and after four stages of library selection and evolution, a synNC termed v4 (version 4, the result after 4 stages of design and evolution) demonstrated that stability in blood was increased by almost 20-fold, and circulation half-life *in vivo* was increased from less

than 5 minutes to 4.5 hours. A key feature of *in vivo* library selection is iteration, which results in the enrichment of characteristics based on the selection scheme (e.g., tumor accumulation). Unfortunately, there seemed to be no association of v4 with any specific tissue type, but it did provide a malleable and exciting means with which to explore tissue targeting. Specifically, we decided to design and finely tune each part of the capsid, which allows us to completely customize both the exterior and interior surfaces of the synNC.

We approached the development of this system for treatment of neuromuscular disorders from two perspectives; first, to identify potential variations that could be incorporated into AAV to improve tissue specificity and second, by using synNCs themselves as a potential therapeutic gene therapy delivery system. For example, AAVs have already been approved for limited use in patients and are the standard delivery method in the field of gene therapy, and variants of AAV capsids can alter tropism. In addition, there already exist methods and infrastructure to produce large quantities of these therapeutics. Conversely, synNCs are synthetic and thus entirely novel to the immune system, making them a potentially safer option for gene therapy delivery, especially if we continue to evolve them so re-dosing isn't an issue. They also have the capability of being continually evolved in a patient-specific manner, allowing for repeated doses while circumventing immunity. Both methods of gene therapy administration show promise in their continued development, with many working to identify protein binders and synNC surface characteristics that are muscle-specific, allowing for more precise and overall safer therapeutic delivery. Therefore, we designed, expressed, and tested two different libraries *in vivo*, a miniprotein display library, and a surface library. The miniprotein display library presents an array of miniproteins on the surface of the synNCs, whereas the surface library are capsids with point mutations on the surface.[92] We evolved both of these libraries over multiple rounds in WT

and tumor-bearing[93] mice to further address the effects of surface libraries on circulation half-life and enriched tissue-targeting (tumor data not shown).

3.3 RESULTS:

3.3.1 In vivo library selection of synNCs with surface mutations and miniprotein binders to alter biodistribution.

To test organ targeting, we first utilized the previously mentioned surface library that was evolved for longer circulation half-life.[92] However, we adjusted the method and performed selection of the synNCs recovered from organs of interest, instead of from just blood. Surface libraries were injected and then allowed to circulate for 20 or 40 minutes over two rounds of selection, then tissue RNA was sequenced following each round of selection. We then calculated the log-enrichment of surface mutants over the unaltered synNC, containing no surface mutations or miniprotein displays, in the spleen, liver, lungs, heart, blood, kidneys, and brain (Fig. 3.1). For the most part, none of the surface mutations significantly altered biodistribution behavior in a unique way (data not included).

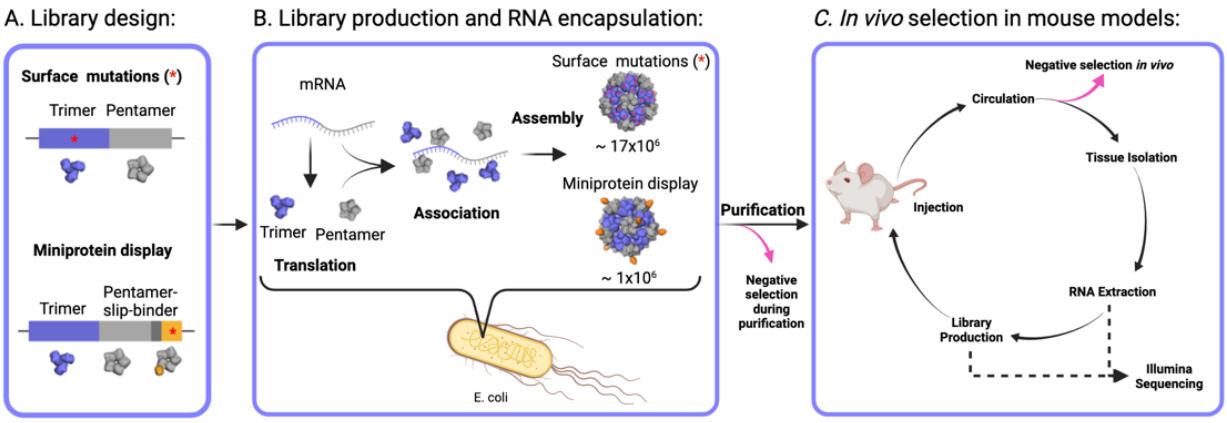

Figure 3.1: Schematic of experimental process for *in vivo* evolution of nucleocapsid library. **A,** The library designs feature surface mutations or mini-protein binders. **B,** synNCs are

synthesized in E. coli via mRNA expression of trimers and pentamers, which then bind their own mRNA and self-assemble into nucleocapsids. **C,** Following production and purification, which inherently de-select for unstable library clones, the samples are injected into an animal model of choice and circulated for 20 or 40 minutes. Then organs were isolated, and RNA is extracted. Enriched mRNA sequences in tissues of interest are then amplified and reproduced for following rounds of selection, with the option to perform Illumina sequencing at every stage.

To produce the synNC miniprotein display library, the Baker Lab in the Institute of Protein Design at the University of Washington provided us with the DNA for a miniprotein library. These miniprotein libraries have been designed to produce stable, folded structures with surface regions that display the typical physiochemical properties of a protein-protein interface. This we then genetically fused to the C-termini of the pentamer subunits under a slip-sequence, ensuring that about 20-40% of the subunits were bound to a miniprotein (Fig. 3.1A).[(94)] The resultant library is composed of ~10^6 different synNC variants that each display a different miniprotein (Fig. 3.1B). In each round of selection, we then sequenced the synNC RNA recovered from the blood, PBMCs, and muscles of healthy mice, as well as from tumors in 4T1 tumor-bearing mice (Fig. 3.1C).

3.3.2 Identification of enriched synNCs in select tissues

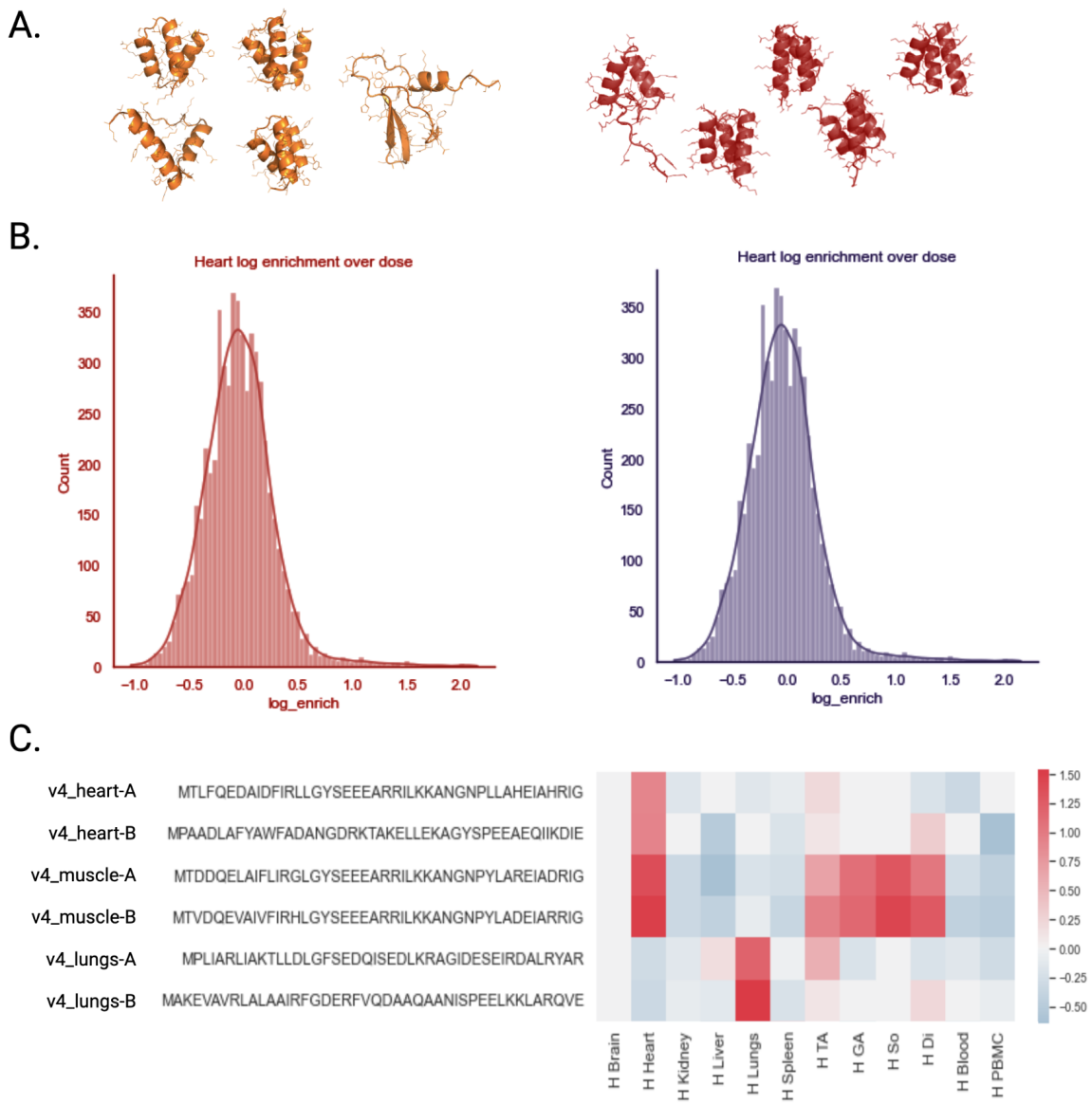

Figure 3.2: synNC sequences enriched in tissue over lowest enrichment in liver. A, Examples of tri-helical bundles found to be enriched in tumor tissue (orange) and heart tissue (red). **B,** Heart (red) and heart+muscle (purple) log enrichment sorted over lowest enrichment in liver. C, Heat map of selected heart, muscle+heart, and lung enriched sequences with which to perform biodistribution studies.

We calculated the log enrichment of sequences identified from chosen organs compared to the library dose that was administered to the mice. Many of the enriched mutants were enriched across all samples sequenced. Using AlphaFold, we then predicted that the enriched miniprotein

surface binders were primarily tri-helical bundles, as we expected (Fig. 3.2A). However, there were also some structures we had not anticipated, for example, single long helix or two helices connected by flexible regions (Figure 3.2A).[95] Notably, in tumor tissue, the highest enriched sequences were tri-helical bundles with exposed hydrophobic residues. We also found that sequences were enriched in a dose-dependent manner, though at a lesser extent, which suggests that sequences may show a specific affinity for organs or organ vasculature.

3.3.3 Biodistribution of most enriched sequences in heart and skeletal muscle.

We analyzed the biodistribution of the two most enriched synNCs in lungs, heart only, and heart+muscle via a fluorescent signal. We altered the interior surface of the synNCs so that they no longer encapsulated mRNA, and instead introduced unique cysteines attached to AlexaFluor 680 molecules. 1 nmol of each of these new synNCs was injected into mice, alongside a v4 control. This was followed by a 30-minute circulation, PBS perfusion, whole-organ imaging, and finally a BCA-fluorescence assay on homogenized organs to measure the AF680 fluorescence per μg protein in each organ sample (n=3 mice per condition).

As expected, the vehicle control showed no signal while the v4 capsid fluoresces in lungs, kidneys, liver, and spleen. Interestingly, the non-targeted v4 control capsid signal was also observed in the diaphragm of mice (Fig. 3.3A). This wA corroborated in the tissues of mice that were injected with v4_lungs-A and v4_lungs-B. The imaging of these lung sequences did not show obvious increased lung fluorescence over v4, but may suggest kidney, liver, and spleen de-targeting. A similar pattern was observed in the mice injected with v4_heart-A and v4_heart-B, where fluorescence can be observed in the kidney, liver, and spleen, but there was significantly

decreased fluorescence in the lungs. Additionally, in the hearts of mice injected with v4_heart-A fluorescence is visible. We again saw an interesting phenomenon with v4_heart-B, where the diaphragm appeared to be slightly enriched. Finally, while v4_muscle-A showed a little fluorescence in the diaphragm and tibialis anterior, v4_muscle-B does not show such promise. However, v4_muscle-B may suggest kidney, liver, and spleen de-targeting, as the fluorescence emitted by these organs was lower than that seen in the v4 control.

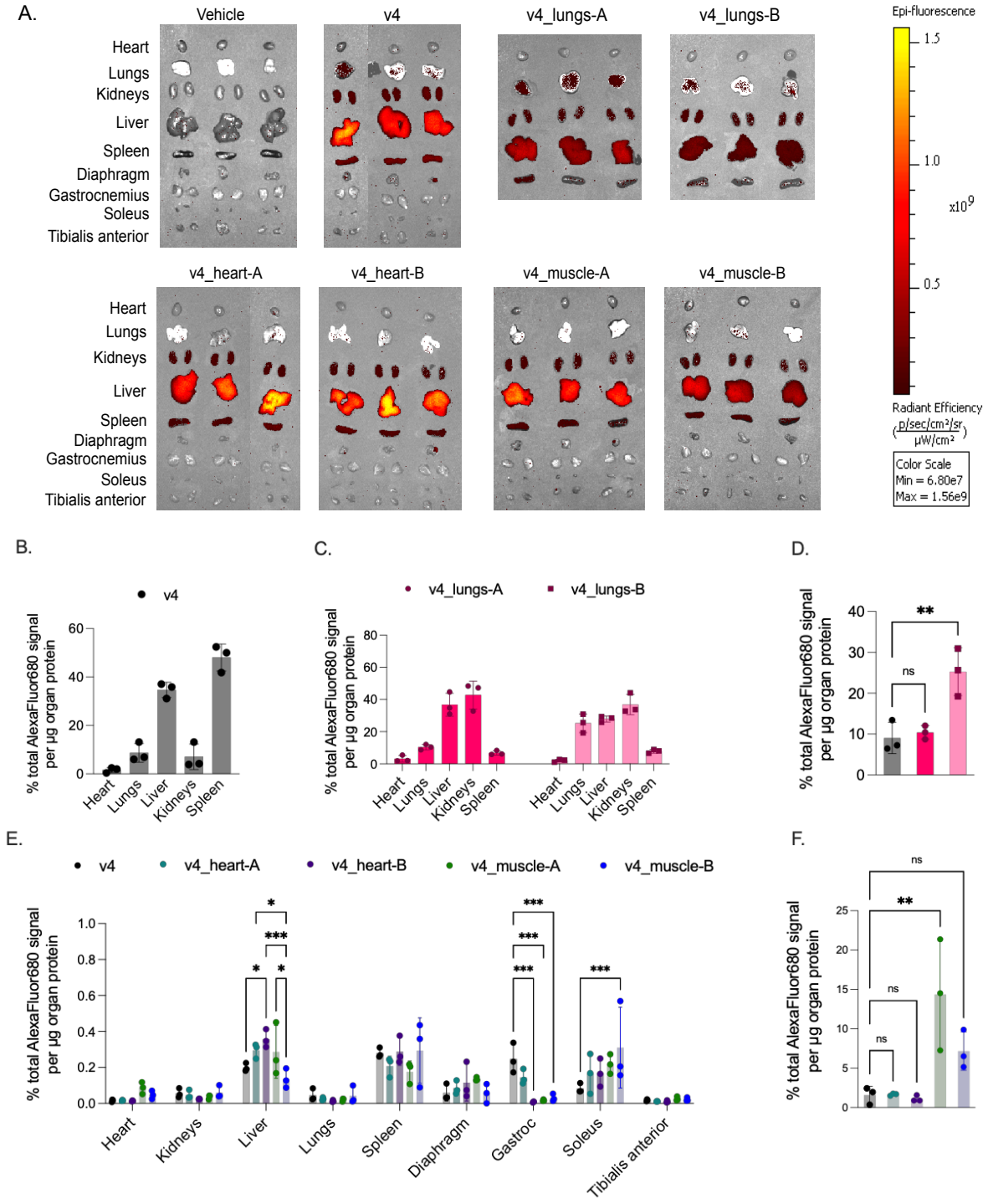

Figure 3.3: Biodistribution and sequence enrichment in tissues. A, Xenogen imaging of tissues collected from mice injected with the vehicle control, the synNC control, or one of six synNCs, with one pair of sequences per tissue: two for lung, to for heart, and two for skeletal muscle. **B-E,** Quantitative analysis of percent fluorescence signal per µg of organ protein. **C,** Comparison of non-targeted control with lung-enriched sequences in lung tissue. **E,** Comparison

of heart tissue with heart and muscle enriched sequences and with non-targeted v4 capsid. Significance indicated by *p=0.05, **p=0.01, ***p=0.001.

When we quantified the fluorescence per μg of organ protein, we saw enrichment of the v4 capsid in the liver and spleen as expected (Fig. 3.3B). The two lung sequences selected had similar patterns, but while v4_lungs-A showed only enrichment in liver and spleen, v4_lungs-B was enriched in the lungs to levels comparable to the liver and spleen (Fig. 3.3C). When examining the enrichment of v4 and the two lung constructs in lung tissue, the significance of the enrichment of v4_lungs-B is further confirmed (Fig. 3.3D). Upon quantification of the heart and heart+muscle hits, we again saw high enrichment in liver and spleen as expected (Fig. 3.3E). Interestingly, we also saw accumulation of the v4 in the gastrocnemius, more so than any designed construct. This was not replicated in other skeletal muscle tissue however, which suggests that this was perhaps a physiological and therefore unreliable result. On the other hand, v4_muscle-B showed significant enrichment in the soleus of treated mice over v4 capsids. The soleus is the only predominantly slow-twitch muscle in the mouse body, implying that muscle fiber composition may be another determining factor in the tissue-targeting abilities of specific nucleocapsids. Finally, when comparing the enrichment of synNC in heart, only v4_muscle-A was significantly increased over v4 (Fig. 3.3F).

3.4 DISCUSSION:

Here, we employed a novel synNC library and evolved it *in vivo* to alter tissue biodistribution for improved therapeutic targeting. We found that specific miniprotein binders displayed on the surface of synNCs can determine the tissue-targeting capabilities of these nanoparticles. While

we initially tested two different libraries, we found that surface mutations on the synNCs did not seem to affect biodistribution. Therefore, specific tissue targeting is likely not determined by simple surface modifications. However, upon further evolution of the miniprotein displaying synNCs, we found specific sequences enriched in desired tissues; information that will play a key role in the development of targeted therapeutics.

SynNCs presenting miniproteins in trihelical bundles are not only uniquely enriched in desired tissues such as tumor, heart, and heart+muscle, but they also present noteworthy sequence motifs. For example, v4_heart-A and v4_muscle-A or -B share 80-82% homology, whereas muscle+v4_heart-A and B share 84% homology. Interestingly however, only v4_muscle-A showed significant enrichment above the non-targeted control in heart. One of the unique motifs of v4_muscle-A is an Asp and a Phe-Leu-Ile-Arg-Gly sequence in the first 14 amino acids of the 44 acid-long sequence, as well as an Arg and Gly in the final 8 amino acids. Conversely, v4_heart-A and v4_muscle-B contain more negatively charged side chains, suggesting that a combination of hydrophobic and positively charged residues in the miniproteins may increase binding to cardiac muscle tissue. The exact mechanism of this targeting behavior necessitates further analysis. It is also important to note that the unique combination of hydrophobic and negatively charged residues seen in v4_muscle-B increased slow-twitch muscle tropism of these capsids, as evidenced by a significant increase in signal enrichment per μg of protein in the soleus (Fig. 3.3E). These data are particularly relevant to the development of therapeutic delivery systems for neuromuscular disorders, as human skeletal muscle is primarily composed of slow-twitch fibers (~70%).

While these sequences have proven effective at targeting specific tissues, the mechanism of this targeting is still unknown. One possibility is that the miniproteins are binding to a specific

ligand or protein on exterior of the muscle cell sarcolemma. We may also have identified binders to specialized endothelial cells in the capillaries of specific tissues. Nucleocapsids may not extravasate, but if the miniproteins are binding to unique endothelial cells, putting these miniproteins on the surfaces of AAVs would greatly increase their targeting and transduction capabilities. Therefore, we can insert these ~45aa miniproteins onto the viral capsid surface as has been shown previously.[96] This lab showed that the position of the peptide insertion and the flanking residues have an effect on vector performance, along with the AAV capsid being used and the tissue type being targeted. This leaves much room for us to further explore the potential of these miniprotein insertions onto AAVs.

The data shown here provide many potential avenues for the further development of delivery vehicles for gene therapy. First, the miniprotein hits selected from biodistribution studies were a limited set of several potential surface binders targeting either heart or heart+muscle tissue, and additional exploration into the biodistribution of other constructs is necessary. Second, the addition of such selected peptide ligands onto the surfaces of AAVs is a well-established protocol and has previously been used as a method to redirect tropism of different serotypes.[97-99] However, incorporation of larger ligands of >34 amino acids into AAV capsids assembly can often significantly reduce vector titers. Third, synNCs and their customizability have shown that they can be designed to effectively target specific tissues, however the transduction efficiency of these capsids remains unknown, though the Baker lab continues to explore their use for therapeutic encapsulation and delivery.

In vivo library selection is a powerful method for therapeutic development because millions of targeting ligands or delivery vehicles can be injected and circulated *in vivo*, and those that exhibit the desired targeting behavior can be identified by linking genotype (recovered

genetic material) to phenotype (e.g., biodistribution). The use of an *in vivo* library development tool shown here and by others[52, 54] has proven to be an efficient and effective way of evolving AAVs and other therapeutic delivery systems.[100] As the field of gene therapy continues to progress, and personalized medicine becomes more standard, both continuing AAV evolution and synNC development may prove crucial to finding the safest, most efficient, and most effective therapeutics for patients facing genetic (i.e. neuromuscular disorders) and acquired diseases (i.e. cancerous somatic mutations).

3.5 MATERIALS & METHODS:

Cloning synthetic nucleocapsid libraries

The I53-50-v4 synthetic nucleocapsid (synNC) genome was PCR-amplified as previously described.[92] Miniproteins were qPCR-amplified by primers that included overlap sites with the synNC genome. Assembly PCR was performed to genetically fuse the miniproteins to the synthetic nucleocapsids. Assemblies were cloned into protein production vectors, electroporated into DH10beta cells, and grown at 37°C on agar-kanamycin plates overnight. Plates were scraped, plasmid DNA was isolated, plasmid DNA was electroporated into BL21-DE* producer cells, and cells were grown at 37°C on agar-kanamycin plates overnight. Bacterial lawns were collected from the plates and used to inoculate large producer cultures for protein production. At both plating steps, bacteria were serially diluted and spotted onto separate agar plates to calculate the approximate library coverage.

Protein production and fluorescent labeling

Proteins were produced and purified as previously described.[92] Briefly, proteins were produced in *E. coli* via IPTG induction or autoinduction, cell pellets were microfluidized, and the supernatant was subjected to immobilized metal affinity chromatography (IMAC). Triton X-114 was used to remove lipopolysaccharides (endotoxin). Samples were incubated with 10 μg/mL RNase H for 10 minutes at room temperature to remove free RNA. Immediately following, size exclusion chromatography (SEC) was performed on a Superose 6 Increase column with PBS. Samples were stored at 4°C. For fluorescent labeling, samples were labeled with maleimide-FITC or maleimide-AlexaFluor680 at 4°C overnight prior to SEC.

Biochemical characterization

Proteins were characterized as previously described.[92] Briefly, molecular weight was analyzed by SDS-PAGE, nucleic acid and protein co-migration and RNase resistance was analyzed by native agarose gel electrophoresis, polydispersity and size were measured by dynamic light scattering (DLS).

RNA isolation, reverse transcription, quantitative PCR, and Illumina sequencing

Samples were stored in Trizol at -80°C. RNA was purified from samples using the RNeasy Mini Kit. Reverse transcription, qPCR, and sequencing on the Illumina MiSeq was performed as described.[92]

In vivo library circulation and organ recovery

4T1 mice were injected with 1 million tumor cells 1-2 weeks before the study and monitored per IACUC protocol. Mice were retro-orbitally injected with 150 μL of sample. After the designated circulation time, mice were euthanized with Avertin overdose and cardiac puncture. Blood was collected from the vena cava. PBS perfusions through the left ventricle were performed. Organs were collected. For fluorescent imaging, organs were imaged with IVIS and homogenized for a BCA plate reader assay. For RNA recovery, organs were snap frozen in liquid nitrogen, ground with a mortar and pestle. A subset of the ground organs was weighed, dissolved in TRIzol, sonicated, and stored at -80 degrees C until RNA extraction. PBMCs were collected by Ficoll separation.

Sequencing analysis

Sequencing analysis was performed by aligning the MiSeq output files with PEAR (a fast and accurate Illumina Paired-End reAd mergeR) and using custom Python scripts.[101] Scripts are available upon request.

Calculating enrichment

Specific sequences are represented by seq. The seq representation is the quotient of the counts of seq in a sample over the total number of sequence reads in the sample. The log(enrichment) of this is the log of seq representation in organ over its representation in the dose.

CHAPTER 4: Conclusions

This culmination of my thesis project has resulted in multiple discoveries regarding the fields of gene therapy and therapeutic delivery systems. In this dissertation, I used biochemical and physiological techniques in combination with novel vector systems and *in vivo* evolution to identify improved gene therapeutics for LGMDR9 and enhanced targeting of therapeutic delivery systems.

4.1 SUMMARY OF FINDINGS: AAV-FKRP gene therapy in wild-type and LGMDR9 mutant mice

In Chapter 2 of this dissertation, I outlined my research and results regarding an AAV gene therapy vector carrying a synthetic FKRP gene for treatment of an LGMDR9 mouse model. This collaborative effort resulted in some key findings that will have major implications in future research toward treating this disease. It also comprises the most comprehensive physiological analysis of gene therapy treatments in LGMD mice as far as we know. First, we found that by removing the untranslated regions of the *FKRP* gene, we saw an increase in FKRP expression *in vitro* following treatment of muscles cells with AAV6-Ck8e-mFkrp. This provided the foundation for the two paths of research we pursued: studying the effects of treatment in older diseased mouse models and comparing of physiological effects of different AAV serotypes carrying this vector on wild type mice.

For the first project, we treated $FKRP^{P448L}$ mutant mice (corresponding to a common mutation in LGMDR9 patients) with the AAV6-Ck8e-mFkrpvector developed during the *in vitro* work, but with the human gene substitution. 10-month-old mice were treated with AAV6-Ck8e-

hFKRP, and extensive physiological assays were performed at 4-, 8-, 12-, and 16-weeks post-injection. While this treatment decreased the effects of exercise-induced impacts and improved overall muscle physiology relative to untreated mutant mice, it did so at lesser levels than have been previously reported. While this is likely an effect of the advanced age at which the mice were treated, it is worth further investigating this discrepancy to identify which factors (i.e. age, dose, AAV serotype, etc…) may be the cause. For the second part of this research, we put the same hFKRP construct (without the untranslated regions) into two different AAV serotypes, AAV9 and AAVMYO1, which have both been shown to increase muscle tropism. We then injected these vectors into healthy wild type mice to parse out potential toxic effects of FKRP overexpression. Physiological analyses were performed on these cohorts at 4-, 6-, 8-, 10-, 12-, 14-, and 18-weeks post injection, all of which confirmed a lack of detrimental effects on treated vs. untreated mice.

These data present critical findings that can enable not only gene therapy treatments for LGMDR9 but can also facilitate efforts to improve gene therapy for other diseases. For example, our data provide further confirmation of the effects of regulatory structures and/or sequences within the untranslated regions of a gene, which could be used to specifically tailor gene expression following gene therapy. If overexpression of a specific gene does have toxic or undesirable effects, its expression could be reduced by with the addition of one of these untranslated regions. Additionally, our generation of safety evidence regarding overexpression of FKRP is a critical step in progressing treatments for LGMDR9 closer to clinical use.

4.2 SUMMARY OF FINDINGS: *In vivo* assessment of synthetic nucleocapsid libraries for enhanced tissue targeting

In chapter 3 of this dissertation, we evolved a synthetic nucleocapsid library bearing miniprotein surface binders to target desired tissues more effectively. This work began with the use of a previously developed library of nucleocapsids which encapsulate their own mRNA and which was created by the Baker lab. We created a new library of these capsids with a library of miniproteins to attach to the surface of these capsids. Following two rounds of *in vivo* evolution of these libraries in mouse models, we narrowed down the library to two miniprotein binder assemblies per tissue of interest based upon enrichment of mRNA within that tissue. These select assemblies were then injected into mice to determine the biodistribution and tissue targeting properties of the chosen capsids. The data confirmed that one of the two assemblies enriched in lungs did target lungs following 30-minute circulation. While neither of the capsids chosen based on heart enrichment appeared in heart tissue, one of the muscle+heart hits was significantly present in cardiac tissue, whereas the other muscle+heart assembly did effectively target slow-twitch muscle. These findings are significant for further development of both AAVs for targeting and safety as well as other synthetic therapeutic delivery systems.

CHAPTER 5: SUPPLEMENTAL FIGURES

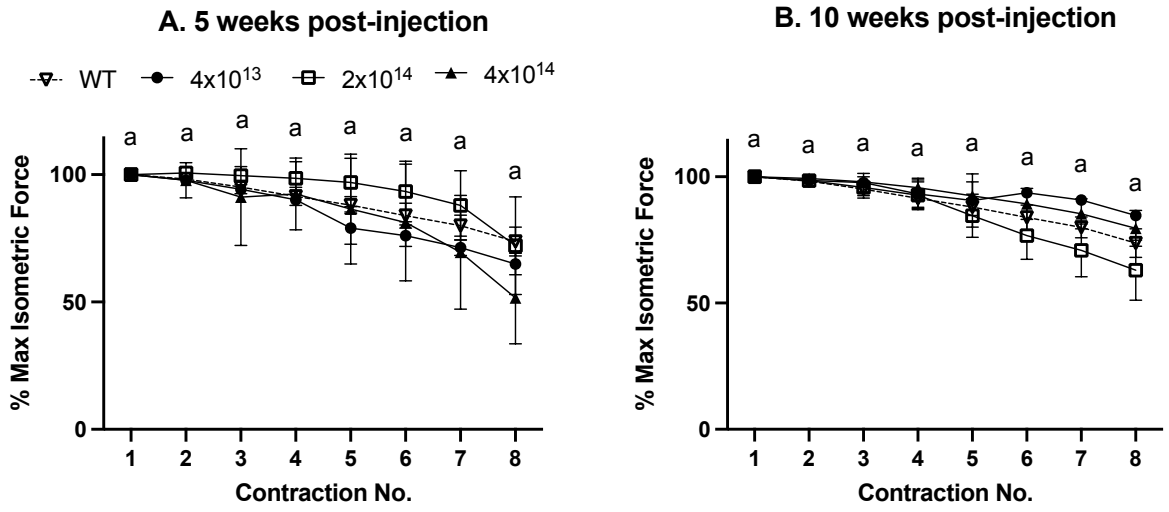

Supplemental Figure 1: AAV-FKRP injection does not increase gastrocnemius muscle susceptibility to contraction-induced injury. Isometric force development in wild-type mice treated with A6.C8hF at doses of $4x10^{13}$, $2x10^{14}$, and $4x10^{14}$ vg/kg. Shown is the percent of maximum isometric force during 8 rounds of gastrocnemius eccentric contractions in situ at 5-weeks (A) and 10-weeks (B) post-injection. No significant differences were observed between any of the groups (shared letter indicate no difference). WT, untreated. (n=3-5)

CHAPTER 6: REFERENCES

1. Tennyson CN, Klamut HJ, Worton RG. The human dystrophin gene requires 16 hours to be transcribed and is cotranscriptionally spliced. Nat Genet. 1995;9(2):184-90.
2. Yue Y, Li Z, Harper SQ, Davisson RL, Chamberlain JS, Duan D. Microdystrophin gene therapy of cardiomyopathy restores dystrophin-glycoprotein complex and improves sarcolemma integrity in the mdx mouse heart. Circulation. 2003;108(13):1626-32.
3. Bengtsson NE, Seto JT, Hall JK, Chamberlain JS, Odom GL. Progress and prospects of gene therapy clinical trials for the muscular dystrophies. Hum Mol Genet. 2016;25(R1):R9-17.
4. Rinaldi C, Wood MJA. Antisense oligonucleotides: the next frontier for treatment of neurological disorders. Nat Rev Neurol. 2018;14(1):9-21.
5. Wang D, Tai PWL, Gao G. Adeno-associated virus vector as a platform for gene therapy delivery. Nat Rev Drug Discov. 2019;18(5):358-78.
6. Dong JY, Fan PD, Frizzell RA. Quantitative analysis of the packaging capacity of recombinant adeno-associated virus. Hum Gene Ther. 1996;7(17):2101-12.
7. Friedrich O, Both M, Gillis JM, Chamberlain JS, Fink RH. Mini-dystrophin restores L-type calcium currents in skeletal muscle of transgenic mdx mice. J Physiol. 2004;555(Pt 1):251-65.
8. Boito CA, Melacini P, Vianello A, Prandini P, Gavassini BF, Bagattin A, et al. Clinical and molecular characterization of patients with limb-girdle muscular dystrophy type 2I. Arch Neurol. 2005;62(12):1894-9.
9. Geguchadze RN, Machen L, Zourelias L, Gallo PH, Passineau MJ. An AAV2/5 vector enhances safety of gene transfer to the mouse salivary gland. J Dent Res. 2012;91(4):382-6.
10. Esapa CT, Benson MA, Schroder JE, Martin-Rendon E, Brockington M, Brown SC, et al. Functional requirements for fukutin-related protein in the Golgi apparatus. Hum Mol Genet. 2002;11(26):3319-31.
11. Esapa CT, McIlhinney RA, Blake DJ. Fukutin-related protein mutations that cause congenital muscular dystrophy result in ER-retention of the mutant protein in cultured cells. Hum Mol Genet. 2005;14(2):295-305.
12. Gerin I, Ury B, Breloy I, Bouchet-Seraphin C, Bolsee J, Halbout M, et al. ISPD produces CDP-ribitol used by FKTN and FKRP to transfer ribitol phosphate onto alpha-dystroglycan. Nat Commun. 2016;7:11534.
13. Cataldi MP, Lu P, Blaeser A, Lu QL. Ribitol restores functionally glycosylated alpha-dystroglycan and improves muscle function in dystrophic FKRP-mutant mice. Nat Commun. 2018;9(1):3448.
14. Briggs DC, Yoshida-Moriguchi T, Zheng T, Venzke D, Anderson ME, Strazzulli A, et al. Structural basis of laminin binding to the LARGE glycans on dystroglycan. Nat Chem Biol. 2016;12(10):810-4.
15. Townsend D. Finding the sweet spot: assembly and glycosylation of the dystrophin-associated glycoprotein complex. Anat Rec (Hoboken). 2014;297(9):1694-705.
16. Michele DE, Barresi R, Kanagawa M, Saito F, Cohn RD, Satz JS, et al. Post-translational disruption of dystroglycan-ligand interactions in congenital muscular dystrophies. Nature. 2002;418(6896):417-22.

17. Kanagawa M, Kobayashi K, Tajiri M, Manya H, Kuga A, Yamaguchi Y, et al. Identification of a Post-translational Modification with Ribitol-Phosphate and Its Defect in Muscular Dystrophy. Cell Rep. 2016;14(9):2209-23.
18. Nishihara R, Kobayashi K, Imae R, Tsumoto H, Manya H, Mizuno M, et al. Cell endogenous activities of fukutin and FKRP coexist with the ribitol xylosyltransferase, TMEM5. Biochem Biophys Res Commun. 2018;497(4):1025-30.
19. Vannoy CH, Xu L, Keramaris E, Lu P, Xiao X, Lu QL. Adeno-associated virus-mediated overexpression of LARGE rescues alpha-dystroglycan function in dystrophic mice with mutations in the fukutin-related protein. Hum Gene Ther Methods. 2014;25(3):187-96.
20. Whitmore C, Fernandez-Fuente M, Booler H, Parr C, Kavishwar M, Ashraf A, et al. The transgenic expression of LARGE exacerbates the muscle phenotype of dystroglycanopathy mice. Hum Mol Genet. 2014;23(7):1842-55.
21. Krag TO, Hauerslev S, Sveen ML, Schwartz M, Vissing J. Level of muscle regeneration in limb-girdle muscular dystrophy type 2I relates to genotype and clinical severity. Skelet Muscle. 2011;1(1):31.
22. Tucker JD, Lu PJ, Xiao X, Lu QL. Overexpression of Mutant FKRP Restores Functional Glycosylation and Improves Dystrophic Phenotype in FKRP Mutant Mice. Mol Ther Nucleic Acids. 2018;11:216-27.
23. Nickolls AR, Bonnemann CG. The roles of dystroglycan in the nervous system: insights from animal models of muscular dystrophy. Dis Model Mech. 2018;11(12).
24. Ervasti JM, Campbell KP. A role for the dystrophin-glycoprotein complex as a transmembrane linker between laminin and actin. J Cell Biol. 1993;122(4):809-23.
25. Praissman JL, Willer T, Sheikh MO, Toi A, Chitayat D, Lin YY, et al. The functional O-mannose glycan on alpha-dystroglycan contains a phospho-ribitol primed for matriglycan addition. Elife. 2016;5.
26. Mercuri E, Brockington M, Straub V, Quijano-Roy S, Yuva Y, Herrmann R, et al. Phenotypic spectrum associated with mutations in the fukutin-related protein gene. Ann Neurol. 2003;53(4):537-42.
27. Sveen ML, Schwartz M, Vissing J. High prevalence and phenotype-genotype correlations of limb girdle muscular dystrophy type 2I in Denmark. Ann Neurol. 2006;59(5):808-15.
28. Keramaris-Vrantsis E, Lu PJ, Doran T, Zillmer A, Ashar J, Esapa CT, et al. Fukutin-related protein localizes to the Golgi apparatus and mutations lead to mislocalization in muscle in vivo. Muscle Nerve. 2007;36(4):455-65.
29. Brockington M, Blake DJ, Prandini P, Brown SC, Torelli S, Benson MA, et al. Mutations in the fukutin-related protein gene (FKRP) cause a form of congenital muscular dystrophy with secondary laminin alpha2 deficiency and abnormal glycosylation of alpha-dystroglycan. Am J Hum Genet. 2001;69(6):1198-209.
30. Xu L, Lu PJ, Wang CH, Keramaris E, Qiao C, Xiao B, et al. Adeno-associated virus 9 mediated FKRP gene therapy restores functional glycosylation of alpha-dystroglycan and improves muscle functions. Mol Ther. 2013;21(10):1832-40.
31. Vannoy CH, Xiao W, Lu P, Xiao X, Lu QL. Efficacy of Gene Therapy Is Dependent on Disease Progression in Dystrophic Mice with Mutations in the FKRP Gene. Mol Ther Methods Clin Dev. 2017;5:31-42.
32. Gicquel E, Maizonnier N, Foltz SJ, Martin WJ, Bourg N, Svinartchouk F, et al. AAV-mediated transfer of FKRP shows therapeutic efficacy in a murine model but requires control of gene expression. Hum Mol Genet. 2017;26(10):1952-65.

33. Chan YM, Keramaris-Vrantsis E, Lidov HG, Norton JH, Zinchenko N, Gruber HE, et al. Fukutin-related protein is essential for mouse muscle, brain and eye development and mutation recapitulates the wide clinical spectrums of dystroglycanopathies. Hum Mol Genet. 2010;19(20):3995-4006.
34. Blaeser A, Awano H, Wu B, Lu QL. Progressive Dystrophic Pathology in Diaphragm and Impairment of Cardiac Function in FKRP P448L Mutant Mice. PLoS One. 2016;11(10):e0164187.
35. Qiao C, Wang CH, Zhao C, Lu P, Awano H, Xiao B, et al. Muscle and heart function restoration in a limb girdle muscular dystrophy 2I (LGMD2I) mouse model by systemic FKRP gene delivery. Mol Ther. 2014;22(11):1890-9.
36. Krag TO, Vissing J. A New Mouse Model of Limb-Girdle Muscular Dystrophy Type 2I Homozygous for the Common L276I Mutation Mimicking the Mild Phenotype in Humans. J Neuropathol Exp Neurol. 2015;74(12):1137-46.
37. Vannoy CH, Leroy V, Lu QL. Dose-Dependent Effects of FKRP Gene-Replacement Therapy on Functional Rescue and Longevity in Dystrophic Mice. Mol Ther Methods Clin Dev. 2018;11:106-20.
38. Kregel CK, Allen DL, Booth FW, Fleshner MR, Henriksen EJ, Musch TI, et al. Resource book for the design of animal exercise protocols.: American Physiological Society; 2006. Available from: http://www.the-aps.org/pa/action/exercise/book.pdf.
39. De Luca A. Use of treadmill and wheel exercise for impact on mdx mice phenotype. TREAT-NMD Activity A07: Accelerate preclinical phase of new therapeutic treatment development [Internet]. 2011; (2.0). Available from: http://www.treat-nmd.eu/resources/research-resources/dmd-sops/.
40. Grange RW. Use of treadmill and wheel exercise to assess dystrophic state. TREAT-NMD Activity A07: Accelerate preclinical phase of new therapeutic treatment development [Internet]. 2011; (1.0). Available from: http://www.treat-nmd.eu/resources/research-resources/dmd-sops/.
41. Bye PT, Esau SA, Walley KR, Macklem PT, Pardy RL. Ventilatory muscles during exercise in air and oxygen in normal men. J Appl Physiol. 1984;56(2):464-71.
42. Mahler DA, Moritz ED, Loke J. Ventilatory responses at rest and during exercise in marathon runners. J Appl Physiol. 1982;52(2):388-92.
43. Bassett DR, Jr., Howley ET. Limiting factors for maximum oxygen uptake and determinants of endurance performance. Med Sci Sports Exerc. 2000;32(1):70-84.
44. Lindstedt SL, Thomas RG, Leith DE. Does peak inspiratory flow contribute to setting VO2max? A test of symmorphosis. Respir Physiol. 1994;95(1):109-18.
45. Spurway NC, Ekblom B, Noakes TD, Wagner PD. What limits VO2max? A symposium held at the BASES Conference, 6 September 2010. Journal of sports sciences. 2012;30(6):517-31.
46. De Luca A, Pierno S, Liantonio A, Cetrone M, Camerino C, Fraysse B, et al. Enhanced dystrophic progression in mdx mice by exercise and beneficial effects of taurine and insulin-like growth factor-1. J Pharmacol Exp Ther. 2003;304(1):453-63.
47. Okano T, Yoshida K, Nakamura A, Sasazawa F, Oide T, Takeda S, et al. Chronic exercise accelerates the degeneration-regeneration cycle and downregulates insulin-like growth factor-1 in muscle of mdx mice. Muscle Nerve. 2005;32(2):191-9.

48. Rocco AB, Levalley JC, Eldridge JA, Marsh SA, Rodgers BD. A novel protocol for assessing exercise performance and dystropathophysiology in the mdx mouse. Muscle Nerve. 2014;50(4):541-8.
49. Maricelli JW, Kagel DR, Bishaw YM, Nelson OL, Lin DC, Rodgers BD. Sexually Dimorphic Skeletal Muscle and Cardiac Dysfunction in a Mouse Model of Limb Girdle Muscular Dystrophy 2i. J Appl Physiol (1985). 2017:jap 00287 2017.
50. High-dose AAV gene therapy deaths. Nat Biotechnol. 2020;38(8):910.
51. Wilson JM, Flotte TR. Moving Forward After Two Deaths in a Gene Therapy Trial of Myotubular Myopathy. Hum Gene Ther. 2020;31(13-14):695-6.
52. Weinmann J, Weis S, Sippel J, Tulalamba W, Remes A, El Andari J, et al. Identification of a myotropic AAV by massively parallel in vivo evaluation of barcoded capsid variants. Nat Commun. 2020;11(1):5432.
53. El Andari J, Renaud-Gabardos E, Tulalamba W, Weinmann J, Mangin L, Pham QH, et al. Semirational bioengineering of AAV vectors with increased potency and specificity for systemic gene therapy of muscle disorders. Sci Adv. 2022;8(38):eabn4704.
54. Tabebordbar M, Lagerborg KA, Stanton A, King EM, Ye S, Tellez L, et al. Directed evolution of a family of AAV capsid variants enabling potent muscle-directed gene delivery across species. Cell. 2021;184(19):4919-38 e22.
55. Lukowski SW, Bombieri C, Trezise AE. Disrupted post-transcriptional regulation of the cystic fibrosis transmembrane conductance regulator (CFTR) by a 5'UTR mutation is associated with a CFTR-related disease. Hum Mutat. 2011;32(10):E2266-82.
56. Lukowski SW, Rothnagel JA, Trezise AE. CFTR mRNA expression is regulated by an upstream open reading frame and RNA secondary structure in its 5' untranslated region. Hum Mol Genet. 2015;24(4):899-912.
57. Leppek K, Das R, Barna M. Functional 5' UTR mRNA structures in eukaryotic translation regulation and how to find them. Nat Rev Mol Cell Biol. 2018;19(3):158-74.
58. Cammas A, Millevoi S. RNA G-quadruplexes: emerging mechanisms in disease. Nucleic Acids Res. 2017;45(4):1584-95.
59. Fay MM, Lyons SM, Ivanov P. RNA G-Quadruplexes in Biology: Principles and Molecular Mechanisms. J Mol Biol. 2017;429(14):2127-47.
60. Salva MZ, Himeda CL, Tai PW, Nishiuchi E, Gregorevic P, Allen JM, et al. Design of tissue-specific regulatory cassettes for high-level rAAV-mediated expression in skeletal and cardiac muscle. Mol Ther. 2007;15(2):320-9.
61. Himeda CL, Chen X, Hauschka SD. Design and testing of regulatory cassettes for optimal activity in skeletal and cardiac muscles. Methods Mol Biol. 2011;709:3-19.
62. Goncalves MA, Janssen JM, Nguyen QG, Athanasopoulos T, Hauschka SD, Dickson G, et al. Transcription factor rational design improves directed differentiation of human mesenchymal stem cells into skeletal myocytes. Mol Ther. 2011;19(7):1331-41.
63. Martari M, Sagazio A, Mohamadi A, Nguyen Q, Hauschka SD, Kim E, et al. Partial rescue of growth failure in growth hormone (GH)-deficient mice by a single injection of a double-stranded adeno-associated viral vector expressing the GH gene driven by a muscle-specific regulatory cassette. Hum Gene Ther. 2009;20(7):759-66.
64. Hu C, Kasten J, Park H, Bhargava R, Tai DS, Grody WW, et al. Myocyte-mediated arginase expression controls hyperargininemia but not hyperammonemia in arginase-deficient mice. Mol Ther. 2014;22(10):1792-802.

65. Muir LA, Nguyen QG, Hauschka SD, Chamberlain JS. Engraftment potential of dermal fibroblasts following in vivo myogenic conversion in immunocompetent dystrophic skeletal muscle. Mol Ther Methods Clin Dev. 2014;1:14025.
66. Blankinship MJ, Gregorevic P, Allen JM, Harper SQ, Harper H, Halbert CL, et al. Efficient transduction of skeletal muscle using vectors based on adeno-associated virus serotype 6. Mol Ther. 2004;10(4):671-8.
67. Gao G, Vandenberghe LH, Alvira MR, Lu Y, Calcedo R, Zhou X, et al. Clades of Adeno-associated viruses are widely disseminated in human tissues. J Virol. 2004;78(12):6381-8.
68. Gregorevic P, Blankinship MJ, Allen JM, Crawford RW, Meuse L, Miller DG, et al. Systemic delivery of genes to striated muscles using adeno-associated viral vectors. Nat Med. 2004;10(8):828-34.
69. Yin FC, Spurgeon HA, Rakusan K, Weisfeldt ML, Lakatta EG. Use of tibial length to quantify cardiac hypertrophy: application in the aging rat. Am J Physiol. 1982;243(6):H941-7.
70. Maricelli JW, Kagel DR, Bishaw YM, Nelson OL, Lin DC, Rodgers BD. Sexually dimorphic skeletal muscle and cardiac dysfunction in a mouse model of limb girdle muscular dystrophy 2i. J Appl Physiol (1985). 2017;123(5):1126-38.
71. Maricelli JW, Lu QL, Lin DC, Rodgers BD. Trendelenburg-Like Gait, Instability and Altered Step Patterns in a Mouse Model for Limb Girdle Muscular Dystrophy 2i. PLoS One. 2016;11(9):e0161984.
72. Mendell JR, Al-Zaidy SA, Rodino-Klapac LR, Goodspeed K, Gray SJ, Kay CN, et al. Current Clinical Applications of In Vivo Gene Therapy with AAVs. Mol Ther. 2021;29(2):464-88.
73. Kishimoto TK, Samulski RJ. Addressing high dose AAV toxicity - 'one and done' or 'slower and lower'? Expert Opin Biol Ther. 2022;22(9):1067-71.
74. Ertl HCJ. Immunogenicity and toxicity of AAV gene therapy. Front Immunol. 2022;13:975803.
75. Bonnemann CG, Belluscio BA, Braun S, Morris C, Muntoni F. A collaborative analysis by clinical trial sponsors and academic experts of anti-transgene SAEs in studies of gene therapy for DMD. Mol Ther. 2022;30(5S1):4.
76. Cheng A, Liu C, Ye W, Huang D, She W, Liu X, et al. Selective C9orf72 G-Quadruplex-Binding Small Molecules Ameliorate Pathological Signatures of ALS/FTD Models. J Med Chem. 2022;65(19):12825-37.
77. Hordeaux J, Buza EL, Jeffrey B, Song C, Jahan T, Yuan Y, et al. MicroRNA-mediated inhibition of transgene expression reduces dorsal root ganglion toxicity by AAV vectors in primates. Sci Transl Med. 2020;12(569).
78. Cao J, Novoa EM, Zhang Z, Chen WCW, Liu D, Choi GCG, et al. High-throughput 5' UTR engineering for enhanced protein production in non-viral gene therapies. Nat Commun. 2021;12(1):4138.
79. Wasala NB, Yue Y, Vance J, Duan D. Uniform low-level dystrophin expression in the heart partially preserved cardiac function in an aged mouse model of Duchenne cardiomyopathy. J Mol Cell Cardiol. 2017;102:45-52.
80. Keramaris E, Lu PJ, Tucker J, Lu QL. Expression of glycosylated alpha-dystroglycan in newborn skeletal and cardiac muscles of fukutin related protein (FKRP) mutant mice. Muscle Nerve. 2017;55(4):582-90.

81. Kregel KC, Allen DL, Booth FW, Fleshner MR, Henrikson EJ, Musch TI. Resource Book for the Design of Animal Exercise Protocols2006.
82. Konopka AR, Harber MP. Skeletal muscle hypertrophy after aerobic exercise training. Exerc Sport Sci Rev. 2014;42(2):53-61.
83. Gehrig SM, Koopman R, Naim T, Tjoakarfa C, Lynch GS. Making fast-twitch dystrophic muscles bigger protects them from contraction injury and attenuates the dystrophic pathology. Am J Pathol. 2010;176(1):29-33.
84. Webster C, Silberstein L, Hays AP, Blau HM. Fast muscle fibers are preferentially affected in Duchenne muscular dystrophy. Cell. 1988;52(4):503-13.
85. Halbert CL, Allen JM, Chamberlain JS. AAV6 Vector Production and Purification for Muscle Gene Therapy. Methods Mol Biol. 2018;1687:257-66.
86. Speakman JR. Measuring energy metabolism in the mouse - theoretical, practical, and analytical considerations. Front Physiol. 2013;4:34.
87. Maricelli J, Bishaw Y, Wang B, Du M, Rodgers BD. Systemic Smad7 Gene Therapy Increases Striated Muscle Mass and Enhances Exercise Capacity in a Dose-Dependent Manner. Hum Gene Ther. 2017.
88. Banks GB, Chamberlain JS. The value of mammalian models for duchenne muscular dystrophy in developing therapeutic strategies. Curr Top Dev Biol. 2008;84:431-53.
89. Ronzitti G, Gross DA, Mingozzi F. Human Immune Responses to Adeno-Associated Virus (AAV) Vectors. Front Immunol. 2020;11:670.
90. Gustafson HH, Olshefsky A, Sylvestre M, Sellers DL, Pun SH. Current state of in vivo panning technologies: Designing specificity and affinity into the future of drug targeting. Adv Drug Deliv Rev. 2018;130:39-49.
91. Munch RC, Janicki H, Volker I, Rasbach A, Hallek M, Buning H, et al. Displaying high-affinity ligands on adeno-associated viral vectors enables tumor cell-specific and safe gene transfer. Mol Ther. 2013;21(1):109-18.
92. Butterfield GL, Lajoie MJ, Gustafson HH, Sellers DL, Nattermann U, Ellis D, et al. Evolution of a designed protein assembly encapsulating its own RNA genome. Nature. 2017;552(7685):415-20.
93. Pulaski BA, Ostrand-Rosenberg S. Mouse 4T1 breast tumor model. Curr Protoc Immunol. 2001;Chapter 20:Unit 20 2.
94. Chevalier A, Silva DA, Rocklin GJ, Hicks DR, Vergara R, Murapa P, et al. Massively parallel de novo protein design for targeted therapeutics. Nature. 2017;550(7674):74-9.
95. Jumper J, Evans R, Pritzel A, Green T, Figurnov M, Ronneberger O, et al. Highly accurate protein structure prediction with AlphaFold. Nature. 2021;596(7873):583-9.
96. Borner K, Kienle E, Huang LY, Weinmann J, Sacher A, Bayer P, et al. Pre-arrayed Pan-AAV Peptide Display Libraries for Rapid Single-Round Screening. Mol Ther. 2020;28(4):1016-32.
97. Michelfelder S, Varadi K, Raupp C, Hunger A, Korbelin J, Pahrmann C, et al. Peptide ligands incorporated into the threefold spike capsid domain to re-direct gene transduction of AAV8 and AAV9 in vivo. PLoS One. 2011;6(8):e23101.
98. Buning H, Srivastava A. Capsid Modifications for Targeting and Improving the Efficacy of AAV Vectors. Mol Ther Methods Clin Dev. 2019;12:248-65.
99. Yu CY, Yuan Z, Cao Z, Wang B, Qiao C, Li J, et al. A muscle-targeting peptide displayed on AAV2 improves muscle tropism on systemic delivery. Gene Ther. 2009;16(8):953-62.

100. Yang L, Jiang J, Drouin LM, Agbandje-McKenna M, Chen C, Qiao C, et al. A myocardium tropic adeno-associated virus (AAV) evolved by DNA shuffling and in vivo selection. Proc Natl Acad Sci U S A. 2009;106(10):3946-51.
101. Zhang J, Kobert K, Flouri T, Stamatakis A. PEAR: a fast and accurate Illumina Paired-End reAd mergeR. Bioinformatics. 2014;30(5):614-20.